HINDCASTING AND FORECASTING OF CLIMATOLOGY FOR GILBERT BAY, LABRADOR: A MARINE PROTECTED AREA

SARA J. BEST

HINDCASTING AND FORECASTING OF CLIMATOLOGY FOR GILBERT BAY, LABRADOR: A MARINE PROTECTED AREA

by

© Sara J. Best

A thesis submitted to the

School of Graduate Studies

in partial fullment of the

requirements for the degree of

Master of Science

Environmental Science Program

Memorial University of Newfoundland

7 March 2011

ST. JOHN'S NEWFOUNDLAND

Abstract

Gilbert Bay is a marine protected area (MPA) on the southeastern coast of Labrador, Canada. The MPA was created to conserve a genetically distinctive population of Atlantic cod, *Gadus morhua*. Future climate change in the region is expected to have an impact on the coastal marine environment and local communities in the future. This thesis presents results from a hindcast and forecasts study of physical oceanographic conditions for Gilbert Bay.

The first section of this thesis examines the interannual variability in atmospheric and physical oceanographic characteristics of Gilbert Bay over the period 1949-2006. The seasonal and interannual variability of the near surface atmospheric parameters are described. Seawater temperature, salinity and sea-ice thickness in winter are simulated with a physical ocean model, the General Ocean Turbulence Model (GOTM). The results of the hindcast model suggest that the atmospheric interannual variability of the Gilbert Bay region is linked to the North Atlantic Oscillation (NAO). A warming trend observed in the subpolar North Atlantic was influenced by the local climate of coastal Labrador during the recent decade of 1995-2005.

The second section of this thesis presents a model forecast of the impact of climate change on the physical conditions within Gilbert Bay over the next century. Climate scenarios from the Intergovernmental Panel on Climate Change (IPCC) Fourth Assessment and the US Climate Change Science Program Project (US CCSP), specifically the Special Report on Emission Scenarios (SRES), were used. Atmospheric parameters and related changes in seawater temperature, salinity and sea-ice thickness in

winter for three SRES are simulated with the GOTM, and are then compared to the hindcast study results. The results suggest that the water column during future winters will become warmer in the second half of the 21st century. In the summer the atmosphere will be warmer and more humid. Cloudiness and precipitation are expected to increase. This will have an impact on the vertical stratification of the water column. The surface mixed layer is expected to become warmer, fresher and much shallower than seen in the past. The stratification below the seasonal thermocline will weaken and vertical mixing will intensify. A significant change in surface sea-ice coverage is also suggested by the forecast. Continuing reduction in sea-ice formation during the winter months as highlighted by the hindcast study is expected to affect living conditions of the neighbouring coastal communities around the bay, specifically by increasing the danger of travelling across the bay. A warming Gilbert Bay ecosystem may be favourable for cod growth, but reduced sea-ice formation during the winter months increases the danger of travelling across the bay by snowmobile.

Acknowledgements

Completing this research would not have been possible without the assistance of many people to whom I would like to express my gratitude.

My co-supervisors, Dr. Entcho Demirov and Dr. Joseph Wroblewski, provided much patience and encouragement. Thank you for providing me with so many opportunities to grow and learn, and helping me receive a well-rounded education. Sarah Lundrigan extracted the NCEP/NCAR reanalysis data for the coordinates of the Gilbert Bay region.

My friends, both near and far, always provided me with a smile and good company. Thank you for knowing I needed it, even when I didn't know.

My parents, Donald and Sheila, and my sister, Donna, always helped me put things in perspective. Thank you for encouraging me to strive to become the best of myself and loving me no matter what. I love you.

The modeling research was supported by the Canadian Foundation for Climate and Atmospheric Sciences. Memorial University of Newfoundland provided a Graduate Studies Fellowship.

Table of Contents

List of Figures

List of Abbreviations

AO Arctic Oscillation

AOI Area of Interest

BUFR Binary Universal Format Representation

CDAS Climate Data Assimilation System

CM Coupled Model

CPC Climate Prediction Center

COSEWIC Committee on the Status of Endangered Wildlife in Canada

DFA Department of Fisheries and Aquaculture, Government of NL

DFO Department of Fisheries and Oceans, Government of Canada

ECMWF European Centre for Medium-Range Weather Forecasts

GFDL Geophysical Fluid Dynamics Laboratory in Princeton, New Jersey

GHG Greenhouse Gases

GISST Global Ice and Sea Surface Temperature Reanalyses

GOTM General Ocean Turbulence Model

GTS Global Telecommunications System

IPCC Intergovernmental Panel on Climate Change

IUCN International Union for Conservation of Nature and Natural Resources

JMA Japanese Meteorological Agency

LMN Labrador Métis Nation

MPA Marine Protected Area

MUN Memorial University of Newfoundland

NAO North Atlantic Oscillation

NCAR National Center for Atmospheric Research in Boulder, Colorado, USA

NCEP National Center for Environmental Prediction in Camp Springs, Maryland, USA

NESDIS National Environmental Satellite Data and Information System

NMC National Meteorological Center

NOAA National Oceanic Atmospheric Administration

SRES Special Report Emission Scenarios

SST Sea Surface Temperature

TOVS Television Infrared Operational Vertical Sounder

UKMO United Kingdom Meteorological Office

US CCSP United States Climate Change Science Program

WMO World Meteorological Organization

Chapter 1: Introduction

1.1 Climate change

Climatology focuses on the description and the analysis of the climate, causes for change in climate variables and the consequences of these changes (McGuffie & Henderson-Sellers, 2005). Climate is the average weather, as described by statistical tests of surface parameters, like precipitation, temperature and wind, over a period of time. The World Meteorological Organization (WMO) defines this time period as 30 years (IPCC, 2007). In studying climatology, both climate variability and climate change are of importance. Climate variability is associated with variations in climatic parameters for a particular region from the mean conditions on all spatial and temporal scales (IPCC, 2007). Studying different spatial scales allows for detection of differences in climatic variables between various regions. Studying temporal scales allows for analysis of climate variability from year to year.

Climate change, however, reflects prolonged change (decadal or longer) in the mean and variability of climatic parameters. Both climate variability and climate change may be a result of natural processes within the climate system, or a result of anthropogenic forcing (IPCC, 2007).

As previously mentioned climatology deals with long-term changes in particular climate variables. Two major influences on coastal regions are the circulation of the ocean, and changes in solar radiation (McGuffie & Henderson-Sellers, 2005). Studying the climate of coastal regions will enhance understanding of current climatic conditions and allow for predictions of the future climate.

The coastal region of particular interest here is that of the southeastern coast of Labrador. This area is located in the Boreal Shield ecozone. Areas located within this ecozone tend to have long, cold winters and short, warm summers. For the southeastern coast of Labrador winter temperatures tend to range between -20 to -1°C, whereas the temperatures during the daily average for the summer months range from 8.5 to 12.5°C (Vasseur & Catto, 2008). Precipitation in this ecozone is found to range from 900 to 2000 mm annually (Vasseur & Catto, 2008; Environment Canada, 1993, 2005a). Sea-ice along the Labrador Sea is said to exhibit significant annual variability, specifically during the winter months (Deser & Holland, 2002). From late fall to spring, the coastal regions of southeastern Labrador experience the formation and duration of sea-ice, specifically landfast ice. Landfast ice tends to be relatively immobile near the coast and extends from the coast as a smooth continuous sheet for a specific period of time (Eicken, 2006; WMO, 1985).

Climate variability over the North Atlantic, and coastal areas like southeast Labrador, are affected by the Labrador Current and the North Atlantic Oscillation (NAO) (Vasseur & Catto, 2008; Catto et al., 2003; Czaja and Frankignoul, 2002).

1.2 The NAO

The NAO refers to alterations in the atmospheric pressure at sea level between the Iceland low and the Azores high (Hurrell et al., 2003; Straile et al., 2003). The NAO index represents the difference between the normalized pressure anomalies for both the Icelandic low and Azores high. A positive NAO index represents a difference in pressure systems where the Azores maximum is higher than normal and the Iceland minimum is lower than usual. A negative NAO index is present when both pressure systems are weaker than usual. In the North Atlantic, climate anomalies associated with the atmosphere and ocean are linked to the NAO index. These anomalies are found to be the greatest during the boreal winter months, particularly March, followed by February and January (Portis et al., 2001). This has an impact on atmospheric variability, causing these climate anomalies to be significantly more intense during this time than other periods in the year (Hurrell et al., 2003).

The changes in the NAO during the winter season have been associated with three topics which are of primary interest for this study: changes in surface air temperature, ocean heat content, and sea-ice coverage (Hurrell et al., 2003). Other atmospheric changes include wind speed and direction, heat and moisture transports, and precipitation (Drinkwater et al., 2003; Hurrell et al., 2003). It is the combination of these atmospheric properties that lead to surface ocean forcing within the water column that affect the temperature and salinity, vertical mixing, circulation patterns and the creation of sea-ice (Drinkwater et al., 2003; Visbeck et al., 2003).

A positive NAO index has been linked to stronger northerly winds over northeastern Canada carrying cold air south, lowering land and sea surface temperatures along the northwest Atlantic Ocean (Hurrell et al., 2003). During a positive NAO index, the boundary of sea-ice extends further south in the Labrador Sea (Deser et al., 2002; Deser et al., 2000; Hurrell et al., 2003). Pack ice, coarse and jagged ice that is often found further offshore than landfast ice, is then driven onshore along the Labrador coast and northeastern Newfoundland. Pack ice could prevent drainage of water from the heads of estuaries, coves and obstruct harbours (Vasseur & Catto, 2008; Catto et al., 2003).

Another important aspect of the NAO is that it strongly correlates to the Arctic Oscillation (AO) which dominates the climate and extent of sea-ice in the Arctic Ocean (Hurrell et al., 2003). The trend in the variability of winter Arctic sea-ice determines the amount of ice in both the Labrador and Greenland Seas.

The NAO is also associated with ecological impacts on ocean ecosystems (Drinkwater et al., 2005), particularly the interannual variability of ecological descriptors found in areas of freshwater and marine systems (Straile & Stenseth, 2007). In the boreal and Arctic regions, winter and early spring play an important role in ecological dynamics (Straile & Stenseth, 2007; Campbell et al., 2005; Sturm et al., 2005). The NAO has the strongest connection with the Northern Hemisphere climate during this time (Straile & Stenseth, 2007; Hurrell et al., 2003; Hurrell, 1995), and because of this, it makes for a reasonable predictor of interannual ecological variability (Straile & Stenseth, 2007). Studies have shown that the NAO index is often a better predictor of ecological processes than local meteorological variables. The NAO indices average out the meteorological conditions over temporal and spatial timescales (Straile & Stenseth, 2007; Hallett et al., 2004) while taking into account different climate parameters like precipitation, wind speed and direction and temperature (Straile & Stenseth, 2007; Stenseth & Mysterud, 2005).

There currently has been little research conducted pertaining to the effect of the NAO on freshwater or estuarine ecosystems of the subpolar North Atlantic. It is theorized that the findings for terrestrial freshwater systems will be different than those freshwater estuarine driven systems. Some of these processes include: temperature, salinity and vertical stratification in the water column.

Marine life is also thought to be affected by the NAO. However, it should be clarified that the biotic life within these coastal and oceanic marine ecosystems in the Northern Hemisphere are not responding directly to the NAO but rather indirectly through alternating patterns within atmospheric and ocean characteristics that are associated with the variability of the NAO (Drinkwater et al., 2003; Ottersen et al., 2001). For instance, living species, from lower trophic levels, such as phytoplankton and zooplankton, to higher levels of life, such as fish, are thought to be indirectly affected by the NAO. Phytoplankton are microscopic plants that are a major resource in the primary production and photosynthetic activity in marine habitats (Drinkwater et al., 2003). It has been shown that phytoplankton show interannual variability as a result of changes in ocean temperature and wind (Drinkwater et al., 2003; Colebrook, 1982); characteristics associated with the NAO (Hurrell, 2003; Straile et al., 2003). Thus, by studying the climatology of freshwater estuarine systems it is possible to assess how biotic life within the marine ecosystems is influenced by the NAO.

1.3 Gilbert Bay, Labrador

Located along the southeast coast of Labrador is the region known as Gilbert Bay. Gilbert Bay is embedded along the coastline and is a freshwater estuarine region. The bay is located in the subarctic region of eastern Canada (Copeland et al., in press). The bay has an area of approximately 82 km^2 with a length of 28 km and width of 1 to 2.5 km (Copeland et al., in press). The water depth of Gilbert Bay is generally shallower than 25 m, but depths reach 60 m in the outer part of the bay (Fisheries and Ocean, 2007; Wroblewski et al., 2007). The majority of its freshwater input comes from the Gilbert

River and the Shinneys River (Figure 1.1) and occurs mostly during the spring thaw (Morris & Green, 2002; Copeland et al., in press). The source of this freshwater is from forested watersheds (Copeland et al., in press). Outlets are located at Williams Harbour Run and the Winnard Tickle (Figure 1.1). Six sills separate seven basins along the main axis of the bay. These sills, which range in depth from 4 to 6.5 m, prevent the water in the bay from flowing directly into the Labrador Sea (Copeland et al., in press; Copeland et al., 2006). The opening of the bay to the Labrador Sea is blocked by islands with the exception of three entrances, all less than 350 m wide (Copeland et al., in press; Copeland et al., 2006; Government of Canada, 2005). This complex bathymetry affects the estuarine circulation. The marine ecosystem in this region is influenced by variations in landfast ice, which occurs during late November to the beginning of May, and vertical stratification (Government of Canada, 2005). During the winter maximum ice thickness is approximately 1 m (Wroblewski, 2008). For the remainder of this thesis, sea-ice will refer to landfast ice unless otherwise stated.

Gilbert Bay is a Marine Protected Area (MPA). The International Union for Conservation of Nature and Natural Resources (IUCN) defines a MPA as, "any area of intertidal or sub-tidal terrain, together with its overlying water and associated flora and fauna, historical and cultural features, which has been reserved by law or other effective means to protect part, or all of the enclosed environment" (Government of Canada, 2005). In Canada, MPAs are established under the Oceans Act of 1997 to conserve commercially important species and protect non-commercial species. This protection extends to endangered, or threatened marine species and their habitats, unique marine habitats, and marine areas of high biodiversity or biological productivity (Jamieson and Levings, 2001).

Gilbert Bay was first declared an Area of Interest (AOI) in October 2000. The Gilbert Bay Steering Committee composed of community leaders, representatives of fishermen's organizations, the Labrador Métis Nation (LMN), Department of Fisheries and Oceans (DFO), Department of Fisheries and Aquaculture (DFA), and Memorial University of Newfoundland (MUN) was formed in 2001 to development a management plan. In 2005, the Minister of Fisheries and Oceans Canada declared Gilbert Bay as the first MPA established in the Canadian subarctic coastal zone (Wrobleski, et al., 2007). Unlike other MPAs, Gilbert Bay is not a harvest refugium or 'no take' reserve (Wroblewski, et al., 2007). The primary reason for Gilbert Bay becoming a MPA is to protect a resident population of Atlantic cod, *Gadus morhua*. These cod are genetically distinguishable from bay cod along the eastern coast of Newfoundland and offshore cod of the Grand Banks (Ruzzante, et al., 2000). Gilbert Bay cod have a reddish or golden-brown colour, a consequence of a carotenoid-rich diet of invertebrates (Wroblewski, et al., 2007). Furthermore, these cod were determined to be a subpopulation of the northern cod metapopulation, which were declared endangered by the Committee on the Status of Endangered Wildlife in Canada (COSEWIC), but still not guarded by Canada's Species at Risk Act (Wroblewski et al., 2007). Conservation of Gilbert Bay cod will help protect the genetic diversity of the northern Atlantic cod metapopulation (Hu and Wroblewski, 2009).

By studying the present climate of Gilbert Bay one can gain an understanding of how climate change may impact the cod population. Furthermore, by studying the changing landfast ice thickness, it is also possible to understand the implications for people living in surrounding communities. This thesis considers how greenhouse gas (GHG) emissions may increase over time and how these emissions may affect the climate of the Gilbert Bay region.

1.4 Purpose of this study

The **purpose** of this thesis is to explore the effects of interannual climate variability on the coastal region of Gilbert Bay, Labrador. The **approach** of the study is based on combining of existing observations (Wroblewski, 2008) and an ocean model to assess the past and future variability in Gilbert Bay. The **objectives** of the study are:

(i) To simulate ocean conditions of Gilbert Bay over the past half century and to compare simulations with available observations.

(ii) To simulate the future features of the Gilbert Bay pertaining to experimental climate change.

(iii) To use the model results from the forecast simulations to identify possible future social and environmental implications of these climate changes.

Two concepts are developed from conducting this research. The first concept involves exploring the time scales and strength of variability in vertical stratifications within Gilbert Bay and how they have changed over the past and how they may possibly change in the future. From these projected changes in stratification the possible effect on phytoplankton blooms, and thus, the overall biological productivity within the bay can be examined. This may impact the Gilbert Bay Atlantic cod population.

The second concept involves examining the sea-ice thickness over time and how it may change in future years. Using the North Atlantic Oscillation (NAO) as a reference for the type of climate that might exist (i.e. colder or warmer climate), it is possible to see how sea-ice formation corresponds to changes in large scale atmospheric processes represented by the NAO index. This will allow one to see if the local climate and sea-ice thickness follows a trend, and if this trend will continue in the future or deviate. This concept is of particular importance to this area of coastal Labrador, as there are communities which are isolated during the winter season. People depend highly on sea-ice as a road for their snowmobiles. Change in the timing of sea-ice formation, duration and thickness will ultimately affect the way of life for many of these people.

1.5 Outline of the thesis

Chapter 2 describes the data and methodology used to conduct the model simulations for the study. Chapter 3 discusses the model run for the hindcast data of Gilbert Bay, chapter 4 discusses the model runs for the future projections of Gilbert Bay and chapter 5 summarizes the research results and provides a discussion.

The results presented in chapter 2 and 3 are published in Best et al. (2011).

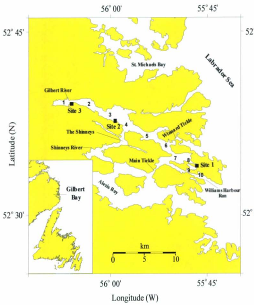

Figure 1. A map of Gilbert Bay, Labrador. The waters of Gilbert Bay connect with the Labrador Sea through Winnard Tickle and Williams Harbour Run, and with Alexis Bay through Main Tickle. Hydrographic stations 1-10 along the main axis of Gilbert Bay and a mooring at Site 1 provided temperature and salinity data for this modelling study.

Chapter 2: Data sources and modelling methodology

A hindcast simulation and three simulations of the future were generated. Sections 2.1 and 2.2 describe the atmospheric forcing and data sources used for the hindcast and model simulations of the future. Section 2.3 describes the oceanographic data that exists for Gilbert Bay. In section 2.4 the model used to run the simulations is described.

2.1 Hindcast atmospheric data

There are currently a number of resources where atmospheric data needed for this study are available. Environment Canada offers historical atmospheric data for areas such as Cartwright, Mary's Harbour, and Port Hope Simpson; all locations of relatively close proximity to the studied region. Atmospheric data from this resource includes such parameters as atmospheric temperature, relative humidity, standard atmospheric pressure and wind direction and speed (Environment Canada, 2010). The Environment Canada data do not extend far enough into the past as is needed for this study. Furthermore, monthly atmospheric data is available for certain years only. For this reason the atmospheric data used as model forcing for the hindcast simulations were taken from the National Center for Environmental Prediction/National Center for Atmospheric Research (NCEP/NCAR) 40-year Reanalysis Project (Kalnay et al., 1996).

The purpose of the Reanalysis Project was to produce a 40-year global record of atmospheric fields to aid in both weather and short-term climate research (Kalnay et al., 1996). The project was initiated in 1991 as an extension to the National Meteorological Center (NMC) Climate Data Assimilation System (CDAS) Project. Since the time it was initiated, the reanalysis project has been expanded to provide over 50 years of global atmospheric data.

The reanalysis system to process and organize the atmospheric data was created at NCEP with aid from the NCEP Environmental Modeling Center, Climate Prediction Center (CPC), the Coupled Model Project, and Central Operations. NCAR carried out most of the data collection and obtained numerous datasets from international sources that were not available through the Global Telecommunications System (GTS), such as atmospheric data from China, Television Infrared Operational Vertical Sounder (TOVS) data, ocean reanalysis data, early global ice and sea surface temperature (SST) reanalyses (GISST), cloud-track winds and rawinsonde data and sea ice data (Kalnay et al., 1996). Sources for these datasets not available by the GTS were the University of Missouri, the National Oceanic Atmospheric Administration's (NOAA)/National Environmental Satellite Data and Information System (NESDIS), the Geophysical Fluid Dynamics Laboratory (GFDL), United Kingdom Meteorological Office (UKMO), the Japanese Meteorological Agency (JMA) and the European Centre for Medium-Range Weather Forecasts (ECMWF) (Kalnay, 1996).

The data were generated through the T62/28-level NCEP global spectral model (equivalent to a horizontal resolution of approximately 210 km and 28 vertical levels) and saved in the WMO's Binary Universal Format Representation (BUFR) (Kalnay et al., 1996). A benefit of using the NCEP/NCAR reanalysis data is that the reanalysis system used to process the data initially preprocessed and compared the collected atmospheric data against climatology statistics to help detect and correct any potential errors in the datasets prior to reanalysis. The preprocessor was also set to establish the surface boundary conditions of data fields such as SST and sea-ice (Kalnay et al., 1996). This is important as the climate of the Gilbert Bay is influenced by the Labrador Sea and severe weather patterns which often originate along the jet stream over the North American continent and propagate towards the North Atlantic.

This procedure provides an estimate of the impact of atmospheric processes over the land and sea on the Gilbert Bay climate by using the NCEP/NCAR dataset. In this way one does not take into account the impact of the local effects of topography and surface properties (sea-ice, land, vegetation, etc.). The NCEP/NCAR Reanalysis Project data was chosen as the data offered is available semi-hourly for an extensive time period for the majority of global coordinates, has been carefully examined and corrected of errors. For this research project six hour reanalysis data from 1949-2006 interpolated for the Gilbert Bay region were used.

2.2 Projections of future atmospheric conditions

Atmospheric data for the future projections were taken from the NOAA's GFDL (Delworth et al., 2006; Geophysical Fluid Dynamics Labratory, 2005). The simulated data for each future projection were generated through the GFDL CM 2.0 Global Coupled Climate Model (Delworth et al., 2006). The coupled climate model is composed of separate atmosphere, ocean, sea-ice, and land component models, which interact through a flux coupler module (Delworth et al., 2006). The horizontal resolution of the CM 2.0 Global Coupled Climate Model (for atmosphere and land) is 2° latitude by 2.5° longitude, with the atmospheric portion of the model having 24 vertical levels (Delworth et al., 2006). The simulated data generated from the CM 2.0 Global Coupled Climate Model represent four climate scenarios: the present climate during the time span 1949-2001 and three scenarios from the Intergovernmental Panel on Climate Change (IPCC) Fourth Assessment and United States Climate Change Science Program (US CCSP) Projects Special Report on Emission Scenarios (SRES): A2 (highest increase in GHG emissions), A1B (moderate increase in GHG emissions) and B1 (lowest increase in GHG emissions) (IPCC, 2007; WMO/UNEP, 2000). These three scenarios were modelled for the century time span 2001-2101. High frequency forcing simulated data were collected for each of the SRES, with the exception of monthly humidity and area cloud fraction simulated data.

2.3 Oceanographic data for Gilbert Bay

A research program was initiated by Memorial University of Newfoundland in the mid-1990s to study the physical oceanographic variability of the Gilbert Bay ecosystem (Wroblewski et al., 2007). Beginning in 1996 seasonal hydrographic surveys of Gilbert Bay were conducted (Wroblewski, 2008). Temperature and salinity profiles were measured at 10 stations established several kilometres apart along the centre axis of the bay (Figure 1.1) using a Seacat SBE19-03 CTD from Sea-Bird® Electronics Inc. Temperature and salinity data used for this study were from a hydrographic station located at a central point within Gilbert Bay (Station 5 in Figure 1.1) which has a water column depth of 65m. Data from 1996 for July 7th and October 4th, from 1997 for March 26th and May 26th and from 2004 for August 13th were utilized for this study. No historical oceanographic data other than that presented in Wroblewski (2008) are presently available for Gilbert Bay. The oceanographic data of Wroblewski (2008) are used to calculate seasonal mean temperatures and salinities of the water column. These data are used to constrain (relaxation of the model simulations towards observations) the temperature and salinity in the bottom layer below 20 to 25 m. Additionally, surface layer salinity for both the hindcast and future projections of the three climate scenarios are constrained by the observations for Gilbert Bay.

The hindcast section of the study also makes use of a time series of ocean temperature that exist for an inlet near the mouth of Gilbert Bay (Wroblewski, 2008). Since October 2003, seawater temperature has been monitored using a VEMCO® data logger positioned at 4 m depth on a mooring located 100 m off a cove beach near Williams Harbour (Site 1 in Figure 1.1). Hourly recording of seawater temperature at this site was maintained through 2004, 2005, 2006 and 2007 (Wroblewski, 2008).

2.4 The model

This study utilizes the General Ocean Turbulence Model (GOTM) (Umlauf et al., 2007). It is a one-dimensional water column model of hydrodynamic and thermodynamic processes in natural waters, with the core of the model computing solutions for the one-dimensional (vertical) versions of the transport equations of momentum, salt and heat (Umlauf et al., 2007). To account for uncertainties in the surface fluxes and lateral transport in the GOTM, temperature and salinity in the surface and bottom layers are constrained through relaxation to observations. Salinity is determined using the following equation:

$$\frac{\partial S}{\partial t} + \omega \frac{\partial S}{\partial z} = \frac{\partial}{\partial z} K_S(v) \frac{\partial S}{\partial z} + \frac{S^{obs} + S(t)}{\tau_S} \qquad (2.1)$$

while temperature is determined from:

$$\frac{\partial T}{\partial t} + \omega \frac{\partial T}{\partial z} = \frac{\partial}{\partial z} K_T(v) \frac{\partial T}{\partial z} + \frac{T^{obs} + T(t)}{\tau_T} \tag{2.2}$$

where $K_S(v)$ and $K_T(v)$ represent the functions of viscosity (v) and τ_S and τ_T represent the relaxation times for salinity and temperature profiles (Umlauf et al., 2007). The relaxation time for salinity and temperature in the bottom layer was set to one month. The surface water flux is corrected through the observed salinity with a relaxation time of three months.

A thermodynamic three layered sea-ice model (Semtner, 1976) was coupled with the GOTM to simulate seasonal evolution of sea-ice. It describes the time-dependent vertical diffusion process that occurs within the ice, modified by effects of internal heating due to penetrating solar radiation and internal storage of heat in brine pockets (Semtner, 1976). The sea-ice model is based on the premise that the ice formed is landfast ice, where snow can accumulate seasonally. During the seasons when there is an accumulation of snow fall, the temperature of the accumulated snow is represented by the following one-dimensional heat equation:

$$(\rho c)_s \frac{\partial T}{\partial t} = \frac{K_s \partial^2 T}{\partial z^2} \tag{2.3}$$

where $K_s = 7.4 \times 10^{-4} \frac{cal}{cm \cdot s \cdot ^\circ C}$ and $(\rho c)_s = 0.165 \frac{cal}{cm^3 \, ^\circ C}$. It is important to note that no change in values occur for when the snow melts as the melting is assumed to occur for a short period of time and during this time conductive fluxes are considered to be minimal (Semtner, 1976).

To represent the temperature of the ice the sea-ice model makes use of the equation:

$$(\rho c)_I \frac{\partial T}{\partial t} = \frac{K_I \partial^2 T}{\partial z^2} \tag{2.4}$$

where $K_I = 4.86 \times 10^{-4} \frac{cal}{cm \cdot s \cdot {}^\circ C}$ and $(\rho c)_I = 0.45 \frac{cal}{cm^3 {}^\circ C}$ to represent constants associated with low temperature ice. The model is set so that one grid point lies in the snow (if present) and two are evenly placed within the ice. Although the thickness of ice will vary, the algorithm is designed to change the resolution accordingly without restricting the time step of the model.

The sea-ice model created by Semtner (1976) also takes into consideration the absorption of penetrating radiation and the increase of trapped brine volume. During periods where there is no snow, penetrating solar radiation is stored in a heat reservoir, representing internal melting within the ice. The radiation energy collected in the heat reservoir is used to keep the surface temperature of the ice from lowering past the freezing point. The overall result is the solar energy radiating at the surface does not cause immediate melting of surface ice during the summer but delays internal cooling during the fall (Semtner, 1976). Thus, the sea-ice model generated by Semtner (1976) was utilized for this study as it should produce relatively accurate formation and melting of landfast ice along Gilbert Bay, Labrador.

The vertical mixing scheme used for this study, within the GOTM, is the k-ε turbulence model by Rodi (1987) (Umlauf et al., 2007; Burchard & Baumert, 1995). This model uses an equation for rate of dissipation to close the system of equations about mean flow characteristics and turbulent kinetic energy (Rodi, 1987; Umlauf et al., 2007).

The model is initialized with the observed winter vertical profiles of temperature and salinity. The GOTM is forced by the heat, momentum and freshwater fluxes between the atmosphere and ocean, and also by the incoming solar radiation (Umlauf et al., 2007). The module makes use of the parameterization for latent and sensible heat fluxes as suggested by Kondo (1975) (Umlauf et al., 2007). The GOTM is restrained by observed salinity and temperature profiles discussed above from hydrographic station 5 (Figure 1.1).

Chapter 3: Interannual variability of physical oceanographic characteristics of Gilbert Bay, Labrador

Utilizing the GOTM (Umlauf et al., 2007) ocean temperature and salinity data from Wroblewski (2008) and atmospheric forcing from the NCEP/NCAR reanalysis were incorporated into the hindcast simulation for the period 1949-2006. This chapter describes the connection of the NAO to the climate of Gilbert Bay, comparing the GOTM model simulation to known observations. This chapter also analyzes and discusses the physical oceanographic variability of Gilbert Bay. Section 3.1 presents a regional analysis of the surface atmospheric parameters over the past 56 years for the period 1949-2006. This period represents the NCEP/NCAR reanalysis atmospheric data currently available for the Gilbert Bay region. In Section 3.2 simulations of surface layer temperature are compared with the observations. Section 3.3 discusses the temporal variability of Gilbert Bay temperature and salinity and ice formation. Section 3.4 summarizes the results of the hindcast study.

3.1 Seasonal variability

Figure 3.1 shows the seasonal variability of four atmospheric parameters for the Gilbert Bay region as generated by GOTM - atmospheric temperature near the sea surface, relative humidity, total cloud cover and total surface heat flux across the air-sea interface. The monthly-mean atmospheric temperature of the Gilbert Bay region computed for 1949-2006 reaches its minimum in February (below -11°C) and reaches its maximum (above 10°C) in July. The temperature is subzero from December to March.

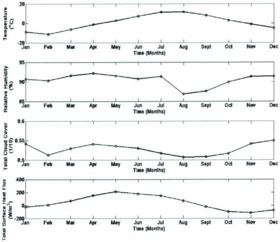

Figure 3.1. Monthly-averaged atmospheric temperature as taken from NCEP/NCAR data for the Gilbert Bay region for 1949-2006 (top panel). Monthly-averaged relative humidity as taken from NCEP/NCAR data for the Gilbert Bay region for 1949-2006 (second panel). Monthly-averaged total cloud coverage as taken from the NCEP/NCAR data for the Gilbert Bay region for 1949-2006 (third panel). Monthly-averaged total surface heat flux as taken from NCEP/NCAR data for the Gilbert Bay region for 1949-2006 (fourth panel).

This is the period when the surface is also ice-covered, which is discussed in more detail later in the thesis. A four month (December to March) period instead of standard three winter months (DJF or JFM) is used due to the fact that the winter at this latitude and longitude is longer than three months.

The humidity and cloud cover in the Gilbert Bay region show similar variability with maximums in December and April and a minimum in late summer (Figure 3.1). High humidity in April is related to the characteristics of local weather and, more specifically, to the advection of humid and cold air from the ocean towards the coastal area.

The heat flux is highest in May, when the sea-ice melts and the waters of the bay become in contact with the atmosphere (Figure 3.1). The contrast of the air-water temperature is highest during this period when the heat flux is strongest. The strongest water cooling occurs in November when the atmosphere is cooling.

The NAO is the dominant mode of regional climate variability, having an impact on atmospheric circulation and air and water characteristics in the Gilbert Bay region. Figure 3.2 shows the winter (December to March) NAO index calculated as the difference of normalized pressure anomaly in Lisbon and Reykjavik (Hurrell & Deser, 2010). These NAO index data were collected from the NCAR Climate and Global Dynamics Climate Analysis Section (National Center for Atmospheric Research, 2009). The NAO index was filtered by using a fourth order Butterword filter with a cut off of three years; represented by the black curve in Figure 3.2. The weather in the Gilbert Bay region is colder and drier during periods of a high positive NAO, and warmer and wetter when the NAO index is negative (Hurrell & Deser, 2010; Drinkwater et al., 2005). The NAO index during the 1950s and 1960s was in a negative phase (Figure 3.2). This was a warm period in the Gilbert Bay region (Figure 3.2). In 1969 the mean temperature for the winter months was above -3°C (Figure 3.2). This is the highest value for the entire period of 1950-2006 in Gilbert Bay. During the time span 1989-1995, the NAO index reached the highest positive index for the period considered in this study (Figure 3.2). This was a cold period in the Gilbert Bay region with the mean air temperatures for the winter season (December-March) of these years falling below -12°C in 1993 (Figure 3.2). The correlation coefficient of the NAO with the mean atmospheric temperature for the winter months (December-March) is $r_{1950\text{-}2006} = -0.7669$ for the period 1950-2006. Calculated over two separate periods, this coefficient is $r_{1950\text{-}1981} = -0.832$ from 1950 to 1981 and has value $r_{1981\text{-}2006} = -0.6286$ from 1981 to 2006.

During the decade from 1995 to 2005, mean air temperature for the winter months shows a warming trend which is not strongly correlated with the NAO (Figure 3.2). The NAO during 1995-2005 was in a positive phase, but the atmosphere was not as cold as in previous winters of positive NAO index. From 1995 to 2005 the mean air temperature for the winter season (December-March) in the Gilbert Bay region increased about 5°C (Figure 3.2). This warming trend has been observed in the subpolar North Atlantic Ocean since 1995 (Marsh et al., 2008).

The model simulations were performed over the period of time from 1949 to 2006. Focus was placed on the biological applications about the thermohaline structure of the water column during anomalously warm and cold years. The most recent model simulations were compared to these two cases. The study focuses on three specific years 1969, 1993 and 2005, for reasons explained below.

The year 1969 was chosen as it was a particularly warm year during a period of negative NAO index that occurred from 1958-1971 (Figure 3.2). This year was also chosen on consideration of the heat flux and sea-ice variability, having the least amount of sea-ice in Gilbert Bay for the period 1949-2006 (discussed in Section 3.3). The year 1993 was chosen as it is one of the coldest years in the subpolar Atlantic within the past five decades and occurs in a period of cold weather as indicated by the NAO index (Figure 3.2). The year 1993 was also chosen with regards to heat flux and sea-ice variability, having the highest amounts of sea-ice in Gilbert Bay for the period 1949-2005 (discussed below in Section 3.3). Finally, the year 2005 was chosen as it has a positive NAO index and occurs at the end of a decadal period of warming (Figure 3.2).

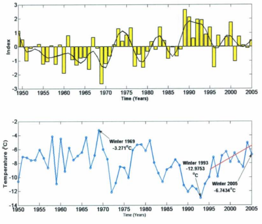

Figure 3.2. NAO index for 1949-2006 as obtained from the NCAR Climate and Global Dynamics Climate Analysis Section (National Center for Atmospheric Research, 2009). Each bar represents the NAO index for the winter months (December-March), while the black line represents the low pass filtered NAO index for the winter months (December-March) (top panel). Mean atmospheric temperature for the winter months (December-March) of Gilbert Bay from 1950-2006 as generated from NCEP/NCAR Reanalysis data. Note the diagonal line along the years 1995-2005 indicating an increase in atmospheric temperature within the decade despite a mostly positive NAO index from 1995-2005 (bottom panel).

3.2 Surface temperature

To determine how the simulated interannual variability of the Gilbert Bay region compared to actual observations, the GOTM simulated seawater temperature was compared to observed hourly near surface seawater temperature from October 2003-October 2007 (Site 1 in Figure 1.1). Figure 3.3 shows good agreement between observations and the model simulations of variability of surface layer temperature during 2004-2007. Gilbert Bay is covered by sea-ice during the winter months, from late December to early May (Wroblewski et al., 2007; Wroblewski, 2008). Both temperature data and model simulation show that the ocean surface becomes ice-free in May of each year. In the model simulation sea-ice melts later than the observations. This is probably related to the lack of representation of ice melting processes in the model. When the sea-ice is thin and the ocean surface is partly ice-free, the solar radiation and turbulent heat fluxes are more efficient in warming the surface layer than represented in the model. The ocean model underrepresents the high frequency variations in the surface layer temperature during the summer. This is related to misrepresentation of some processes of surface heat exchange in this season. While the air temperature over the land warms during the summer, the near surface air masses from the Labrador Sea remain cold during this whole season. The surface atmospheric forcing has coarse time and spatial resolution and does not represent correctly the night time cooling and local transport of cold air from the sea towards the land. Thus in the simulations, the modelled summer temperature is colder than observations (Figure 3.3). These differences between model and data aside, the model reasonably represents spring warming, formation of the surface

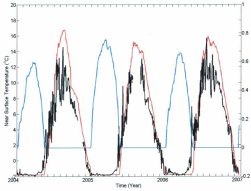

Figure 3.3. Annual sea-ice thickness (blue line) and near surface ocean temperature (red line) simulated by the GOTM compared to observed (at 4m depth) ocean temperature (black line) from mooring station at Site 1 (Figure 1) in Gilbert Bay for 2004-2007. There are periods in fall 2004 and in summer 2005 where no observational temperature data were gathered at the mooring site.

mixed layer and deepening of the mixed layer until the end of winter. These processes are described in detail below.

3.3 Interannual variability of sea-ice, temperature and salinity

The simulated sea-ice thickness in Gilbert Bay from 1949-2007 is shown in Figure 3.4. The winter maximum of sea-ice thickness throughout this period shows a significant interannual variability. Periods of high sea-ice thickness occurred during portions of the early seventies, eighties and early nineties where the NAO index was positive (Figure 3.2). The sea-ice formation was particularly strong in the year 1993 when the thickness reached over 1.2 m. Periods of lesser sea-ice and short periods of sea-ice duration occurred in the late 1960s, 1970s and the most recent years since year 2000. In the year 1969 the sea-ice had a winter maximum thickness of less than 0.4 m (Figure 3.4). These periods of low sea-ice thickness and duration, particularly the year 1969, can be explained by the variability of the surface atmospheric forcing. In the year 2005 the maximum thickness of sea-ice reached slightly over 0.6 m (Figure 3.4), which is lower than expected for a positive NAO index year. This is due to a decadal warming period after 1995.

While the mechanism of this warming in the subpolar North Atlantic is not still clear, it appears that the regime of interannual variability in the region usually related to the NAO was changed. The NAO has a period between 5 to 10 years (Figure 3.2) that generates variations in the atmospheric characteristics with this period. The last 10 years of the studied period show a continuous trend of warming which does not correlate with the NAO index. Hence, focus was placed on the variability of Gilbert Bay in three typical

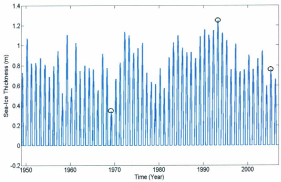

Figure 3.4. Annual formation and melting of sea-ice in Gilbert Bay for 1949-2007 as modelled by the GOTM using both NCEP/NCAR Reanalysis data and observational ocean data from Wroblewski (2008). The graph represents the formation and decrease of landfast sea-ice for each year from 1949-2007. The peaks on the graph represent the maximum sea-ice thickness for each year. The circle placed above the peaks for the years 1969, 1993 and 2005 highlight the difference in maximum sea-ice thickness between warm year 1969, cold year 1993 and the more recent year 2005.

cases of atmospheric stress: warm weather for low NAO index (1969), cold weather for a high NAO index (1993) and recent warming of the subpolar North Atlantic (2005).

The seasonal variability in vertical mixing is an important factor for the vertical transport of dissolved nutrients in the bottom waters upwards towards the euphotic layer to support phytoplankton production (Hu & Wroblewski, 2009). In early spring when the ice begins to melt, fresher water is placed at the surface, resulting in a stratification of the water column (Clarke et al., 2001; Tang, 1991). This water column of intense mixing is confined within a thin 5 to 7m surface layer. This is approximately the depth of penetration of the solar radiation in the seawater (Gosse & Wroblewski, 2004). Later in the year this mixed layer deepens down during autumn and reaches its greatest depths during next winter. A main contributor to this mixing is buoyancy convection. It is driven by surface heat loss due to atmospheric cooling (Hurrell et al., 2003; Straile et al., 2003). Another source for vertical mixing is the surface and bottom shear. Finally, the surface salinity flux can increase due to the salt rejection in the water column from sea-ice formation (Hurrell et al., 2003; Lazier et al., 2001; Clarke et al., 2001). It is the combination these factors that causes the mixed layer to become colder and denser, causing convection in the mixed layer down into the depths of the water column (Hurrell, et al., 2003; Lazier et al., 2001; Clarke et al., 2001).

This seasonal evolution of the surface layer of intense mixing is observed during the entire simulation, but reveals some important variations from year to year (Figure 3.5). These are mainly related to the interannual changes in atmospheric forcing and the duration of the coverage of the surface by sea-ice.

In the cold year 1993, the surface heat loss triggers intensive vertical mixing in the beginning of the winter from January to mid-March (Figure 3.5). In the spring of 1993 the ice-free surface is warmed and a thermocline forms in May (Figure 3.5), which later deepens in autumn and again reaches the bottom of the basin during winter.

Similar seasonal variability of the vertical mixing is observed in the warm year 1969. However, the winter was relatively warm and the sea-ice duration was shorter (Figure 3.4), thus the period of time when the surface water was exposed to the surface cooling was longer (Figure 3.5). Also, the thermocline formed earlier in the spring of 1969 than in 1993, beginning in mid-April, and the seasonal thermocline deepened faster than in 1993 (Figure 3.5). The year 2005 highly resembled the warm year 1969. Again, like 1969 the sea-ice duration was shorter (Figure 3.4) and thus it experienced a longer period of surface cooling and the thermocline also formed earlier than the year 1993, appearing in early April (Figure 3.5).

The temporal variability of the salinity and temperature shown in Figures 3.6 and 3.7 is reflected in the seasonal variations of the intensity of vertical mixing. Unlike the near surface temperature of Gilbert Bay (Figure 3.3) which responds fairly quickly to air temperature, deeper depths of the bay show longer-period fluctuations (Straile et al., 2003; Livingstone, 1993). For instance, during the summer the water column below the thermocline, or hypolimnion, has temperatures that are attained at the end of the winter season (Straile et al., 2003; Robertson & Ragotzkie, 1990; Hondzo & Stefan, 1993; Livingstone, 1993). In Gilbert Bay the seasonal thermocline forms in the spring and then deepens down to the bottom in autumn. The surface layer in spring is fresh and saltier by the end of summer.

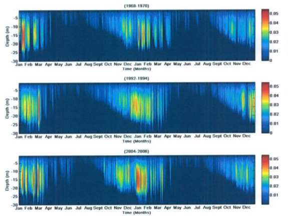

Figure 3.5. Vertical diffusivity seasonal variability for 1968 and 1969 (top panel); 1992 and 1993 (middle panel); 2004 and 2005 (bottom panel). These figures represent the vertical mixing for the years 1969 (a warm year), 1993 (a cold year) and 2005 (a cold year at the end of a decadal warming period) as generated by the GOTM using both NCEP/NCAR Reanalysis data and observational ocean data from Wroblewski (2008). Note the magnitude and duration of vertical mixing in 1993, which are greater and longer than the magnitude and duration for 1969 and 2005.

During the cold winter of 1993 the water column homogenized down to the bottom in mid-December and remained well mixed until late June – early July when the sea-ice melted (Figures 3.6, 3.7). The vertical stratification formed in the spring was very strong due to the low salinity of the surface layer (Figure 3.6), a result linked to the extensive formation of sea-ice the previous winter (Figure 3.4).

For the warm year 1969 (Figures 3.6, 3.7) the homogenized water did not form until early January and the water column remained well mixed until late May – early June. The salinity and temperature stratifications in the spring and summer of 1969 (Figures 3.6, 3.7) were much weaker than in 1993. This facilitated the vertical mixing in the spring and summer of 1969, when the seasonal thermocline deepened much faster than in 1993.

There appear to be similarities of the recent year 2005 to the warm year 1969. The duration of the homogeneous water column is shorter than in 1993, occurring from early January to early June (Figures 3.6, 3.7). The stratifications of both salinity and temperature (Figures 3.6, 3.7) in 2005 were also weaker than the cold year 1993.

The time variability of the thermohaline structures in cold and warm years is illustrated (Figures 3.8, 3.9) in terms of salinity and temperature anomalies. During the spring and summer of cold year 1993 the salinity (Figure 3.8) and temperature (Figure 3.9) of the surface layer and thermocline show negative anomalies, indicating a fresher and colder surface layer and thermocline than average. The stratification is stronger than usual. In warm years (Figures 3.8; 3.9) the stratification in spring and summer is weaker providing favourable conditions for more intense vertical mixing. An interesting aspect is the difference between the temperature anomalies in year 1969 (Figure 3.9) and 2005

(Figure 3.9). Both years are warm and stratification weaker than usual. However, there is one major difference between these years – the salinity anomaly below the halocline and in the deep layer in 2005 (Figure 3.8) is lower than average and temperature below the thermocline (Figure 3.9) is warmer than average. Additionally, salinity in the surface layer is much higher than usual. In 2005 the stratification is weaker than in two previous examples, 1969 and 1993.

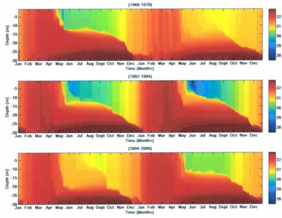

Figure 3.6. Seasonal variability of salinity (psu) for 1968 and 1969 (top panel); 1992 and 1993 (middle panel); 2004 and 2005 (bottom panel). These figures represent the salinity profiles for the years 1969 (a warm year), 1993 (a cold year) and 2005 (a cold year at the end of a decadal warming period) as generated by the GOTM using both NCEP/NCAR Reanalysis data and observational ocean data from Wroblewski (2008). Note the duration and stratification for each year. 1969 and 2005 show a longer halocline duration that is less stratified than in the year 1993.

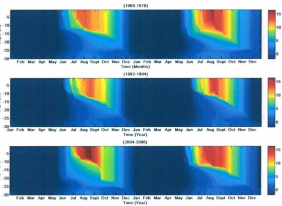

Figure 3.7. Seasonal variability of temperature (°C) for 1968 and 1969 (top panel); 1992 and 1993 (middle panel); 2004 and 2005 (bottom panel). These figures represent the temperature profiles for the years 1969 (a warm year), 1993 (a cold year) and 2005 (a cold year at the end of a decadal warming period) as generated by the GOTM using both NCEP/NCAR Reanalysis data and observational ocean data from Wroblewski (2008). Note the duration and stratification for each year. 1969 and 2005 show a longer thermocline duration that is less stratified than in the year 1993.

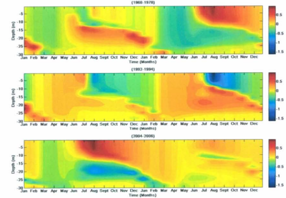

Figure 3.8. Seasonal variability of salinity (psu) anomaly for 1968 and 1969 (top panel); 1992 and 1993 (middle panel); 2004 and 2005 (bottom panel). These figures represent the salinity anomalies for the time period 1949-2006, highlighting the anomalies for the years 1969 (a warm year), 1993 (a cold year) and 2005 (a cold year at the end of a decadal warming period) as generated by the GOTM using both NCEP/NCAR Reanalysis data and observational ocean data from Wroblewski (2008). Note the surface layer for 1969 shows a positive anomaly, indicating a saltier surface layer than average. 1993 shows a negative anomaly, indicating a fresher surface layer than average. 2005 shows a negative anomaly, indicating a colder surface layer than average. Also note now the gradients are weaker for the years 1969 and 2005 as compared to 1993.

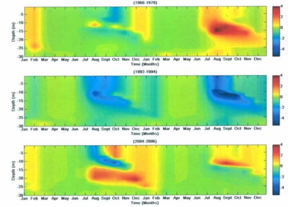

Figure 3.9. Seasonal variability of temperature (°C) anomaly for 1968 and 1969 (top panel); 1992 and 1993 (middle panel); 2004 and 2005 (bottom panel). These figures represent the temperature anomalies for the time period 1949-2006, highlighting the anomalies for the years 1969 (a warm year), 1993 (a cold year) and 2005 (a cold year at the end of a decadal warming period) as generated by the GOTM using both NCEP/NCAR Reanalysis data and observational ocean data from Wroblewski (2008). The surface layer for 1969 shows a positive anomaly, indicating a warmer surface layer than average. 1993 shows a negative anomaly, indicating a colder surface layer than average. 2005 shows a negative anomaly, indicating a colder surface layer than average. The gradients are weaker for the years 1969 and 2005 as compared to 1993.

3.4 Summary

Four atmospheric parameters of the Gilbert Bay region were described for the period 1949-2006. Results indicate that Gilbert Bay is connected to characteristic trends, being linked to the NAO. The impact of the surface forcing variability on the seawater properties of Gilbert Bay were also described for 1949-2006. In particular the temperature and salinity seasonal evolution was examined for three years: 1969 (a negative NAO index year), 1993 (a positive NAO index year) and 2005 (a positive NAO year). In the warm year 1969 sea-ice was thinner during the winter period (Figure 3.4), the stratification in the spring and summer was weaker and the vertical mixing in these seasons were more intense than in the cold year 1993. The warm weather in the year 1969 and cold weather in the year 1993 were caused by variability in the atmospheric circulation related to the NAO oscillations, while the year 2005 did not indicate this link to the NAO.

Although the NAO index is positive in 2005, Gilbert Bay exhibited characteristics similar to the warm year 1969 (Figure 3.2). The variability of water characteristics in 2005 may be considered as an example of the response of the water column to decadal warming (Figure 3.2). The longer term warming trend led to stronger erosion of the thermocline than in 1969. Sea-ice formation has been decreasing the past decade (Figure 3.4) and the salinity of the surface layer has been increasing (Figures 3.6, 3.8). This can be considered a change in the environmental conditions of marine life in Gilbert Bay. These changes in climate over the last decade may be due to regional warming. Current positive NAO trends are associated with North Atlantic SSTs and stratospheric cooling due to greenhouse gases (Cohen & Barlow, 2005). There is also the possibility that this decadal warming, seen independent of the NAO index, could be a direct response to global warming.

Chapter 4: A climate sensitivity study of Gilbert Bay, Labrador: Regional projection of IPCC climate scenarios

The ocean temperature and salinity data from Wroblewski (2008) and atmospheric data from the NCEP/NCAR reanalysis project were used in the previous study of the physical oceanographic variability of Gilbert Bay. With the use of the GOTM, the study showed that the oceanographic conditions within the bay are affected by the NAO, with the exception of the period 1995-2005 which experienced a decadal period of local warming unrelated to the NAO.

To gain insight on the future climate conditions of the coastal region and what impact these changes may have on the marine ecosystem of the bay, the present study utilizes the GOTM, ocean data from Wroblewski (2008) and atmospheric parameters generated by the CM 2.0 Global Coupled Climate Model (Delworth et al., 2006). The objective is to analyze future climate scenarios from the IPCC Fourth Assessment and US CCSP Projects, specifically the SRES. The climate conditions suggested by these three future climate scenarios are compared to the hindcast climate conditions of the Gilbert Bay region presented in Chapter 3. The preliminary analysis of the IPCC present day simulations demonstrate that they do not predict accurately the phase and amplitude of the NAO relaxed interannual variability of the atmosphere (Tristan Houser, personal communication). At the same time these simulations provide an accurate knowledge of the major trends in climate characteristics of the atmosphere and ocean. Hence, in this study the connection between the NAO and the three SRES, along with any possible future changes in the NAO, are not examined as further data would be required to accurately predict such information. By comparing the three SRES to the hindcast climate scenario, we study the major long term trends in the Gilbert Bay climate characteristics in the next 50 to 100 years. Section 4.1 describes the three future climate scenarios, and how they differ between each other. Section 4.2 discusses the potential uncertainty in the future climate simulations. In section 4.3 a brief analysis is given of the changes in the atmospheric parameters between the future scenarios and the hindcast scenario. Section 4.4 discusses predicted changes in the oceanic variability of sea-ice formation, temperature and salinity for the three future climate scenarios over the next century, focusing particularly on the last year of the model simulation, 2100. Section 4.5 summarizes the results and changes in climate as predicted by the IPCC future projections.

4.1 The three climate scenarios

The three climate scenarios are taken from the IPCC Fourth Assessment and US CCSP Projects SRES. The purpose of these scenarios is to help analyze how technological change, environmental, demographic and socio-economic development may affect greenhouse gas (GHG) emission trends in the future (IPCC, 2007; WMO/UNEP, 2000). Using the three climate scenarios within this study will help determine if an increase in GHG emissions will have an impact on the Gilbert Bay region. If so, to what extent will different levels of increase in GHG emissions cause change to the timing, duration and magnitude of atmospheric and ocean processes.

The SRES consist of four storylines: A1, A2, B1 and B2. Each storyline describes differently the connection between the emission driving forces and their evolution (IPCC, 2007; WMO/UNEP, 2000). Together these storylines generate 40 scenarios, which are divided amongst six scenario groups; three groups within A1 and one group each within A2, B1 and B2 (IPCC, 2007; WMO/UNEP, 2000). The three groups within A1 each describe alternative energy technologies development (IPCC, 2007; WMO/UNEP, 2000).

Each climate scenario involves a large number of characteristics such as world population growth, economic development, and technological change (IPCC, 2007; Environment Canada, 2005; WMO/UNEP, 2000); driving forces of GHG and sulphur emissions (IPCC, 2007; WMO/UNEP, 2000). For this reason, their plausibility or feasibility should not be considered solely on the basis of an extrapolation of current economic, technological, and social trends (IPCC, 2007; Environment Canada, 2005; WMO/UNEP, 2000). Emissions are aggregated into four world regions and global totals. In the scenarios no feedback effect of future climate change on emissions from biosphere and energy has been assumed (IPCC, 2007; WMO/UNEP, 2000).

The three climate scenarios chosen from the SRES for this study come from the A1, A2 and B1 storylines. They are scenarios A1B, A2 and B1. Each represent three different possible GHG emission trends for the future, with the A2 scenario having the greatest emissions of GHG, the A1B scenario having the next highest level of GHG emissions, and the B1 scenario having the lowest emissions of GHG (Figure 4.1). Both the A1B (moderate increase in GHG emissions) and B1 (lowest increase in GHG emissions) scenarios begin to degrease in GHG emission after the year 2050.

The storyline for the A2 scenario, with the highest GHG emissions level, is based on a theme of self-reliance and preservation of local identities (Environment Canada, 2005). There exists a high population growth and the economic development is mainly regionally oriented. Per capita economic growth and technological change are more separated and slower than in other SRES scenarios (Environment Canada, 2005).

The A1B scenario, with a moderate level of GHG emissions, is also known as the 720 ppm stabilization experiment. The A1 scenario group has explored variations in energy systems most explicitly and hence covers the largest part of the scenario distribution. This scenario is a median between both A2 (highest increase in GHG emissions) and B1 (lowest increase in GHG emissions) scenarios, where there is a quick economic growth, low population growth and a strong effort made towards efficient technologies. The A1B scenario technology change refers to use of a balance between fossil fuel and non-fossil fuel sources (Environment Canada, 2005).

Finally, the B1 scenario, which has the lowest level of GHG emissions, is also known as the 550 ppm stabilization experiment. The storyline indicates a low global population growth and fairly quick changes in the economy toward a service and information economy and an implication of a clean and resource-efficient technology. This storyline places much emphasis on economic, social and environmental sustainability solutions (Environment Canada, 2005).

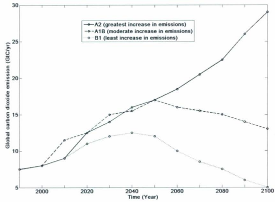

Figure 4.1. Global carbon dioxide (CO_2) emissions (GtC/yr) for the IPCC and US CCSP Projects SRES A2, A1B and B1. The three climate scenarios represent different levels of carbon dioxide emissions with A2 having the highest emissions of CO_2, A1B having a moderate increase in CO_2 and B1 having the lowest increase in CO_2. Note both A1B and begin to decrease in CO_2 emissions after the year 2050.

4.2 Assessment of model uncertainty in IPCC simulations

To analyze the future scenarios and how the different levels of GHG emissions may affect Gilbert Bay, first it was necessary to determine how realistic the simulated data representing the SRES A2 (highest increase of GHG emissions), A1B (moderate increase of GHG emissions) and B1 (lowest increase of GHG emissions) scenarios were with regards to interannual and seasonal variability of the climate. The IPCC simulated data from the NOAA's GFDL CM2 Global Coupled Climate Model were compared to the NCEP/NCAR reanalysis atmospheric data, as the NCEP/NCAR reanalysis data represent the atmospheric parameters of the Gilbert Bay region. The atmospheric temperature, relative humidity and total cloud cover for the period 1949-2001 was compared between the NCEP/NCAR reanalysis and the NOAA's GFDL CM2 Global Coupled Climate Model present climate scenario.

To compare the atmospheric temperatures of each set, the average monthly temperature was calculated for the period 1949-2001. Temperatures from the NCEP/NCAR reanalysis are higher than temperatures from the CM2 Global Coupled Climate Model (Figure 4.2). The bias in the CM2 Global Coupled Model temperature calculated for the Gilbert Bay is highest in January at approximately 9°C and lowest in May and October, at approximately 3°C. Colder CM2 Global Coupled Model temperatures may be linked to an equatorward contraction of the oceanic subtropical gyre circulations within the model when the atmosphere and oceans were coupled (Delworth et al., 2006). The monthly mean bias (Figure 4.2) was removed from the each of the future climate scenarios generated by GFDL CM2 Global Coupled Model.

To compare the relative humidity of each set, the average monthly relative humidity was calculated for the period 1949-2001. Relative humidity from the NCEP/NCAR reanalysis is higher than the humidity in the modelling set from the GFDL CM2 Global Coupled Model (Figure 4.3) during the spring (March to May) and late fall to early winter (October to December). However, during the mid-winter (January to February) and the summer-early fall (June to September) the relative humidity in the CM2 Global Coupled Model dataset is significantly higher than in the NCEP/NCAR reanalysis dataset. The bias in the CM2 Global Coupled Model for the relative humidity done for the Gilbert Bay is the greatest during the months of August and November with differences in humidity at approximately 4.5% and 6.3%. The bias is lowest in March and May with differences in relative humidity less than 1%. The increase of relative humidity during summer and decrease in relative humidity during fall from the CM2 Global Coupled Model was taken into account during the analysis of the three SRES.

The total cloud cover of each modeling set was also compared, calculating the average monthly total cloud cover for the period 1949-2001 (Figure 4.4). The total cloud cover from the GFDL CM2 Global Coupled Model was significantly higher than the NCEP/NCAR reanalysis for all months, with differences in cloud cover ranging at approximately 0.4. Difference in total cloud cover is the lowest for

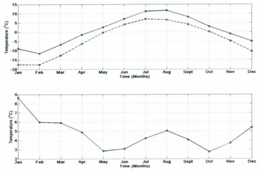

Figure 4.2. Monthly-averaged atmospheric temperature of the Gilbert Bay region for 1949-2000. The figure indicates greater monthly averaged temperatures for the NCEP/NCAR Reanalysis data (solid line) than the GFDL CM2 Global Coupled Climate Model simulated data (dashed line) (top panel). The temperature correction applied to GFDL CM2 Global Coupled Climate Model IPCC scenarios. The black line represents the difference in monthly-averaged atmospheric temperature (NCEP/NCAR Reanalysis dataset minus GFDL CM2 Global Coupled Climate Model simulated data) for the period 1949-2001 (bottom panel).

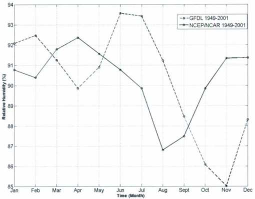

Figure 4.3. Monthly-averaged relative humidity of the Gilbert Bay region for 1949-2001. The figure indicates greater monthly averaged relative humidity for the NCEP/NCAR Reanalysis data (solid line) than the GFDL CM2 Global Coupled Model simulated data (dashed line). Note the differences between the two datasets during the different seasons.

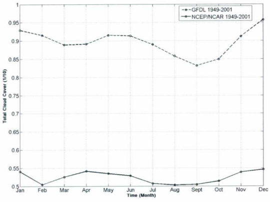

Figure 4.4. Monthly-averaged total cloud cover of the Gilbert Bay region for 1949-2001. The figure indicates greater monthly averaged total cloud cover for the NCEP/NCAR Reanalysis data (solid line) than the GFDL CM2 Global Coupled Climate Model simulated data (dashed line). Note the significant increase in total cloud coverage for the GFDL CM2 Global Coupled Climate Model simulated dataset.

the month of September, at approximately 0.33. The increase of total cloud cover in the GFDL data was taken into account during the analysis of the SRES.

4.3 Predicted changes in the atmospheric characteristics in Gilbert Bay

The atmospheric parameters of the hindcast scenario and the three future climate scenarios were compared for this study. This was done not only to show how the climate changed over time in the Gilbert Bay region, but also to show the link between the atmospheric parameters and GHG emission trends. Figures 4.5 to 4.8 show the seasonal variability of three atmospheric parameters – near surface atmospheric temperature, relative humidity, and total cloud cover. The compared characteristics are monthly mean atmospheric parameters calculated over a 51 year period. For the hindcast these characteristics are calculated for 1955-2006 and for the climate scenarios are calculated for 2050-2101.

All scenarios show warming of climate conditions for the Gilbert Bay region as GHG emissions also increase, with the mean air temperature for the winter months (December-March) for all three forecasting scenarios showing an increase in temperature for the period 2001-2101 (Figure 4.5). The linear fits shown in Figure 4.5 were calculated for each of the SRES by centering at the year 2051and scaling the x-data (year) using the following formula:

(4.1)

where μ is the year 2051, thus giving the following linear regressions for each SRES where y represents temperature: $y_{A2} = 0.0687z - 4.5433$, $y_{A1B} = 0.0509z - 4.2251$ and $y_{B1} = 0.0488z - 4.9214$. The linear regressions indicate that the A2 scenario (highest increase in GHG emissions) shows the greatest increase in temperature, at 0.0687°C/year over the course of the century, followed by the A1B scenario (moderate increase in GHG emissions) at 0.0509 °C/year and finally the B1 scenario (lowest increase in GHG emissions) at 0.0488°C/year.

Figure 4.6 compares the monthly average atmospheric temperature between the hindcast scenario for the period 1955-2006 and the three climate scenarios, A2 (highest increase in GHG emissions), A1B (moderate increase in GHG emissions) and B1 (lowest increase in GHG emissions). The monthly averaged change is strongest in the A2 (highest increase in GHG emissions) scenario and weakest in the B1 (lowest GHG emissions) scenario, thus indicating once again that the increase in temperature is linked to the increase of GHG emissions. The temperature for all four scenarios are subzero from December to March, however both the A2 (highest increase of GHG emissions) and A1B (moderate increase in GHG emissions) scenarios show a warmer temperature for January than the hindcast study. In winter (February) the warming is approximately 4°C in the A2 (highest increase in GHG emissions) scenario, 3°C in the A1B (moderate increase in GHG emissions) scenario and 2°C in the B1 (lowest increase in GHG emissions) scenario. During the summer months, the SRES simulations do show warming from the hindcast. The month of August shows the greatest amount of change for each scenario during summer with warming at approximately 4°C in the A2 (highest increase in GHG emissions), 4°C in the A1B (moderate increase in GHG emissions) and 3°C in the B1 (lowest increase in GHG emissions) scenarios.

Relative humidity for the hindcast scenario shows variability with maximums occurring during February and April (Figure 4.7). High humidity during April is related to the characteristics of local weather and more specifically to the advection of humid and cold air from the ocean towards the coastal area. The forecasting scenarios show an interesting difference from the hindcast. Although the range of the relative humidity is similar for all four scenarios, there is an increase in humidity from January to February in all three climate scenarios and a decrease in humidity for September to December. This is opposite of the hindcast scenario. Humidity for the forecasting scenarios is also greater from June to August. These changes in relative humidity are linked to the bias between the NCEP/NCAR and GFDL CM2 Global Coupled Model generated dataset as noted in section 4.2. Thus results discussed in section 4.4 pertaining to changes in ocean variability in sea-ice, temperature and salinity are reflective of a climate with increases in relative humidity as discussed above. Relative humidity for the period 2001-2101 do suggest an increase for all three climate scenarios when compared to the hindcast scenario, but due to the bias indicated in section 4.2, timing and magnitude of when this increase occurs is uncertain.

All three forecasting scenarios show significantly higher amounts of cloud cover than the hindcast scenario. The total cloud cover for the hindcast scenario ranges between 0.5 to 0.6 while the total cloud cover for the SRES ranges between 0.8 to 1.0 (Figure 4.8), which indicates an increase in precipitation. All the SRES indicate a total cloud cover maximums for January, May and December and total cloud cover minimum for September. The hindcast scenario also indicates a total cloud cover maximum for December. This significant increase in total cloud cover is linked to the bias between the NCEP/NCAR and GFDL CM2 Global Coupled Model generated dataset as noted in section 4.2. Results discussed in section 4.4 pertaining to changes in ocean variability in

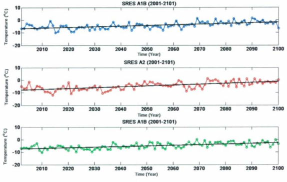

Figure 4.5. Mean atmospheric temperature for the period 2001-2101 during winter months (December-March) of the Gilbert Bay region for: SRES A1B (moderate increase in GHG emissions) (top panel); SRES A2 (highest increase in GHG emissions) (middle panel); SRES B1 (lowest increase in GHG emissions) (bottom panel). The simulated atmospheric temperature for each SRES was taken from the GFDL CM2 Global Coupled Climate Model. The black line on each panel represents the linear regression for that SRES.

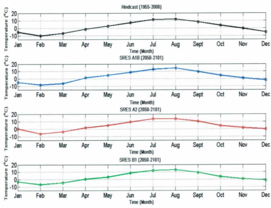

Figure 4.6. Monthly-averaged atmospheric temperature of the Gilbert Bay region for: Hindcast (1955-2006) (top panel); SRES A1B (moderate increase of GHG emissions) (2050-2101) (second panel); SRES A2 (highest increase in GHG emissions) (2050-2101) (third panel); SRES B1 (lowest increase in GHG emissions) (2050-2101) (bottom panel). The atmospheric temperature used to calculate the monthly-averaged atmospheric temperature for the hindcast scenario was taken from the NCEP/NCAR Reanalysis data, while the monthly-averaged atmospheric temperature for each SRES was calculated using simulated data taken from the GFDL CM2 Global Coupled Climate Model.

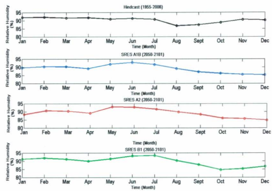

Figure 4.7. Monthly-averaged relative humidity of the Gilbert Bay region for: Hindcast (1955-2006) (top panel); SRES A1B (moderate increase in GHG emissions) (2050-2101) (second panel); SRES A2 (highest increase in GHG emissions) (2050-2101) (third panel); SRES B1 (lowest increase in GHG emissions) (2050-2101) (bottom panel). The relative humidity used to calculate the monthly-averaged relative humidity for the hindcast scenario was taken from the NCEP/NCAR Reanalysis data, while the monthly-averaged relative humidity for each SRES was calculated using simulated data taken from the GFDL CM2 Global Coupled Climate Model.

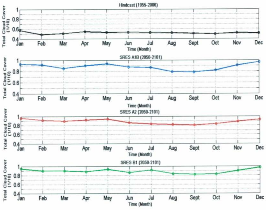

Figure 4.8. Monthly-averaged total cloud cover of the Gilbert Bay region for: Hindcast (1955-2006) (top panel); SRES A1B (moderate increase in GHG emissions) (2050-2101) (second panel); SRES A2 (highest increase in GHG emissions) (2050-2101) (third panel); SRES B1 (lowest increase in GHG emissions) (2050-2101) (bottom panel). The total cloud cover used to calculate the monthly-averaged total cloud cover for the hindcast scenario was taken from the NCEP/NCAR Reanalysis data, while the monthly-averaged total cloud cover for each SRES was calculated using simulated data taken from the GFDL CM2 Global Coupled Climate Model.

sea-ice, temperature and salinity are reflective of a climate with significant cloud coverage as discussed above. Due to the bias indicated in section 4.2, the timing and magnitude of when this increase occurs is uncertain. The cloud cover is used in calculation of the surface heat flux. It has the greatest importance on the surface long wave radiation. The positive bias reflected in the SRES cloud cover simulations result in a positive bias of surface net heat flux. This is uncertainty related to a numerical scheme of cloud parameterization in the GFDL CM2 Global Coupled Model.

It can be concluded that the most important change predicted in the three IPCC scenarios for the Gilbert Bay is that as GHG emissions increase a warming of the atmospheric temperature between 3 to 5°C, strong increase in the humidity, cloudiness and precipitation occur.

4.4 Predicted changes in the ocean variability forced with three IPCC scenarios

In this section, the temporal variability of Gilbert Bay temperature and salinity and ice formation in winter are compared between the hindcast scenario and the forecasting scenarios.

4.4.1 Predicted changes in sea-ice thickness and duration

The simulated sea-ice thickness in Gilbert Bay for each of the three climate scenarios is shown in Figure 4.9 for the period 2001-2101. All three scenarios show a decrease of the sea-ice thickness and duration at the end of the 21st century. This decrease is associated with the overall warming of the atmosphere with increasing temperatures and humidity, particularly during the winter season (Figure 4.5). There is a decrease in the cooling of the water column which prolongs the time needed to cool the water column enough for landfast ice to form. This period of rapid cooling of the water column also does not last as long. The decrease in thickness is strongest in the A2 (highest increase in GHG emissions) and A1B (moderate increase in GHG emissions) scenarios. The sea-ice formation for A1B (moderate increase in GHG emissions) scenario (Figure 4.9) shows the greatest amount of interannual variability having years of very little to no sea-ice formation and years where sea-ice thickness levels ranged between 0.8 to 1.0 m. Scenario A2 (highest increase in GHG emissions) shows a generally lower range of sea-ice thickness (0.4 to 0.7 m) over the course of the century with years of no sea-ice formation, while scenario B1 (lowest increase in GHG emissions) shows the slowest rate of decline with every year over the course of the century, except 2099, having some sea-ice.

The maximum sea-ice thickness occurs at a different year for each scenario, with A1B (moderate increase of GHG emissions) occurring in 2015 at 0.9940 m, A2 (highest increase in GHG emissions) occurring in 2065 at 0.8962 m and B1 (lowest increase in GHG emissions) occurring in 2023 at 0.9506 m. An interesting insight is the sea-ice thickness for the year 2100. Although each scenario shows an overall decline in ice sea-thickness over time, scenario A1B (moderate increase in GHG emissions) shows a greater sea-ice thickness than seen in 2005 (Figure 3.4). The sea-ice thickness for 2005 was slightly above 0.7 m, an anomalously warm year for present climate. Both A2 (highest increase in GHG emissions) and B1 (lowest increase in GHG emissions) scenarios show less sea-ice for this year.

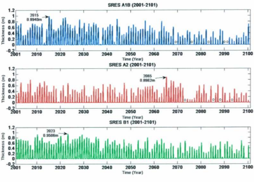

Figure 4.9. Annual sea-ice thickness in Gilbert Bay for: A1B (moderate increase in GHG emissions) scenario (2001-2101) (top panel); A2 (highest increase in GHG emissions) scenario (2001-2101) (middle panel); B1 (lowest increase in GHG emissions) scenario (2001-2101) (bottom panel). The graphs represent the formation and decrease of landfast ice for each year from 2001-2101 as generated by the GOTM using simulated atmospheric data from the GFDL CM2 Global Coupled Climate Model and observational ocean data from Wroblewski (2008). The peaks on the graph represent the maximum sea-ice thickness for each year. The figure highlights the difference in maximum sea-ice thickness between the SRES A2, A1B and B1. Note the scenarios with greater increases in GHG emissions show multiple years of no sea-ice formation (i.e. A2 and A1B scenarios).

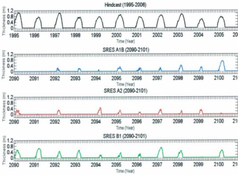

Figure 4.10. Annual sea-ice thickness in Gilbert Bay for the hindcast scenario (1995-2006) (top panel); A1B (moderate increase in GHG emissions) scenario (2090-2101) (second panel); A2 (highest increase in GHG emissions) scenario (2090-2101) (third panel); B1 (lowest increase in GHG emissions) scenario (2090-2101) (bottom panel). The graphs represent the formation and decrease of landfast ice over a decade as generated by the GOTM. The hindcast landfast ice profile was generated using the NCEP/NCAR Reanalysis data and observational ocean data from Wroblewski (2008), while the SRES landfast ice profiles were generated using simulated atmospheric data from the GFDL CM2 Global Coupled Climate Model and observational ocean data from Wroblewski (2008). The peaks on the graph represent the maximum sea-ice thickness for each year. The figure highlights the difference in maximum sea-ice thickness and duration of sea-ice between the hindcast and SRES A1B, A2 and B1. Note how scenario B1 (lowest increase in GHG emissions) has the closest the resemblance to the hindcast scenario.

Figure 4.10 compares the duration of sea-ice and thickness of the hindcast scenario (1995-2006) to the three SRES (2090-2101). This shortened duration is again due to the less intense and shortened period of cooling of the water column due to the increased atmospheric temperatures linked to increasing GHG emissions. The decrease in duration is strongest for the A2 (highest increase in GHG emissions) scenario, followed by the A1B (moderate increase in GHG emissions) and finally the B1 (lowest increase in GHG emissions) scenarios. During the period 2090-2101 duration of sea-ice is significantly shortened from mid-December to late May as seen in the hindcast scenario, to February-March for most years of the A2 (highest increase in GHG emissions) and A1B (moderate increase in GHG emissions) scenarios and February-April for the B1 (lowest increase in GHG emissions) scenario. The B1 (lowest increase in GHG emissions) scenario appears to be the 'best case' scenario with thickness and duration of sea-ice having the closest resemblance to the hindcast scenario.

4.4.2 Predicted changes in temperature and salinity

The temporal variability of the salinity and temperature are shown in Figures 4.11 and 4.12. Figure 4.11 shows the salinity depth profiles for the hindcast scenario for the years 2004 and 2005 for all three forecasting scenarios for the years 2099 and 2100. Comparing the profiles of the three future projections for the year 2100 to the present climate for 2005, a warm year due to a decadal warming period as noted in the hindcast study, significant changes are seen. These changes are a response to the atmospheric changes emissions described in section 4.3. The warm and humid atmosphere, a result of increasing GHG emissions, causes reduction of the time duration of winter cooling. The ice melts in mid March-April and the seasonal halocline forms one to two months earlier than in the hindcast. In the SRES the halocline is quite shallow due to increased precipitation. Thus, the salinity remains low at 16-24 psu in the SRES A2, 19 to 24 psu in the SRES A1B and 20 to 25 psu in the SRES B1 for the span mid-April to mid-July. For comparison of salinity in summer mixed layer in the hindcast is between 29 to 32 psu.

Figure 4.12 shows the temperature depth profiles for the hindcast scenario for the years 2004 and 2005 for all three forecasting scenarios for the years 2099 and 2100. Comparing the hindcast to all three climate scenarios one can see that the thermocline is much shallower in summer for the three future projections, with the depth of the mixed layer remaining under 5 to 7m in summer. The reason for this is the very shallow and strong halocline, due to intense precipitation from increasing temperatures (Houghton et al., 2001) and high humidity in the warm season. The result is a stronger water flux, weaker evaporation, and latent heat loss. Scenarios where the GHG emissions were higher projected warmer temperatures within the water column surface, or thermocline, than did the scenario with less intense emissions. The summer temperatures increase 3 to 4°C in the A2 (highest increase in GHG emissions) and A1B (moderate increase in GHG emissions) climate scenarios with temperatures of 14 to 19°C. The B1 (lowest increase in GHG emissions) scenario more closely resembles summer temperatures of the hindcast at 13 to 16°C. This close resemblance in surface temperatures within the water column between the hindcast and B1 (lowest increase in GHG emissions) scenarios may be due to the decrease in GHG emissions after the year 2050; a result of well-developed sustainability solutions towards reducing carbon emissions (Environment Canada, 2005).

The time variability of the thermohaline structures in the future projections is illustrated (Figures 4.13, 4.14) in terms of salinity and temperature anomalies. Comparing the future projections for the year 2100 to the year 2005 (Figures 4.13, 4.14) there appears to be a decrease in salinity at the surface layer and the duration of this salty layer for all three scenarios as compared to the present climate during the summer months. This is due to the increase in precipitation due the change in total cloud cover for each SRES. The SRES show slightly positive anomalies in the top surface layer during the summer months. One important difference from the hindcast is the reduced magnitude of seasonal variability in all modelled SRES. It is a result from weaker surface winter cooling in this experiment and less intense vertical salt and heat fluxes in summer.The intensity of vertical mixing for the A2 (highest increase in GHG emissions), A1B (moderate increase in GHG emissions) and B1 (lowest increase in GHG emissions) scenarios show some similarity with the hindcast. Seasonally, for each scenario, the mixing is strongest in winter months and weakest in summer. However, comparing the vertical diffusivity there appears to be a significant difference in the magnitude and duration between the hindcast scenario and forecasting scenarios. The hindcast clearly shows seasonal evolution of vertical mixing starting in the early fall and increasing in depth and magnitude during the late fall until early spring when sea-ice begins to melt. The water column began to homogenize down near the bottom in November, reaching the bottom in January where it remained well mixed until mid March to April when the sea-ice melted (Figures 4.11, 4.12).

The three forecasting scenarios show a significant decrease in the magnitude and duration of vertical mixing (Figure 4.11). All SRES show a decrease of 0.02 m^2/s of mixing during portions of the winter season. This may be due to a decrease in sea-ice formation and duration which contributes to less salt expelling into the water column and a more gradual cooling of the water column surface which decreases buoyancy convection; both contributors to vertical mixing (Hurrell, 2003; Straile et al., 2003; Lazier, 2001, Clarke et al., 2001; Tang, 1991). The A1B (moderate increase in GHG emissions) and B1 (lowest increase in GHG emissions) scenarios show the closest similarity to the hindcast scenario with intense mixing occurring from February to March. Vertical mixing from the surface than begins again in the fall increasing in depth and magnitude. The A2 (highest increase in GHG emissions) show little to no vertical mixing for the year 2100, a result of increasing GHG emissions.

A new element in the vertical mixing of the SRES is the intensification of vertical mixing in the bottom layer during the summer season. The physical changes are related to the reduced stability of the seasonal thermocline in the water column. In the climate scenarios the seasonal thermocline is relatively shallow, being less than 5 to 7 m surface layer where intense mixing occurs. Thus, solar radiation penetrates beneath the surface mixed layer. It warms locally the water and reduces the vertical stratification. The mixing of warmed and salty water with colder and fresh water residing at or below the thermocline increases the density causing cabling instability. This mixing is effective in early spring when the thermocline is shallow and water below the thermocline is weakly stratified.

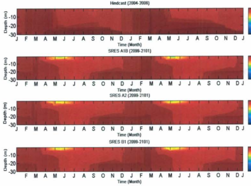

Figure 4.11. Seasonal variability of salinity (psu) for: Hindcast (2004-2006) (top panel); SRES A1B (moderate increase in GHG emissions) (2099-2101) (second panel); SRES A2 (highest increase in GHG emissions) (2099-2101) (third panel); SRES B1 (lowest increase in GHG emissions) (2099-2101) (bottom panel). These figures represent the salinity profiles for the hindcast and the A2, A1B and B1 scenarios as generated by the GOTM. The hindcast temperature profile was generated using the NCEP/NCAR Reanalysis data and observational ocean data from Wroblewski (2008), while the SRES temperature profiles were generated using simulated atmospheric data from the GFDL CM2 Global Coupled Climate Model and observational ocean data from Wroblewski (2008). Note the difference in duration and depth of the halocline for all three climate scenarios.

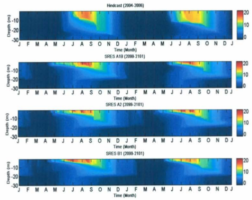

Figure 4.12. Seasonal variability of temperature (°C) for: Hindcast (2004-2006) (top panel); SRES A1B (moderate increase in GHG emissions) (2099-2101) (second panel); SRES A2 (highest increase in GHG emissions) (2099-2101) (third panel); SRES B1 (lowest increase in GHG emissions) (2099-2101) (bottom panel). These figures represent the temperature profiles for the hindcast and the A2, A1B and B1 scenarios as generated by the GOTM. The hindcast temperature profile was generated using the NCEP/NCAR Reanalysis data and observational ocean data from Wroblewski (2008), while the SRES temperature profiles were generated using simulated atmospheric data from the GFDL CM2 Global Coupled Climate Model and observational ocean data from Wroblewski (2008). Note the difference in duration and depth of the shallower thermocline for all three climate scenarios as compared to the hindcast.

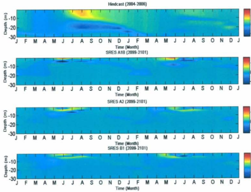

Figure 4.13. Seasonal variability of salinity (psu) anomaly for: Hindcast (2004-2006) (top panel); SRES A1B (moderate increase in GHG emissions) (2099-2101) (second panel); SRES A2 (highest increase in GHG emissions) (2099-2101) (third panel); SRES B1 (lowest increase in GHG emissions) (2099-2101) (bottom panel). These figures represent the salinity anomalies for the hindcast and the future scenarios as generated by the GOTM. The hindcast temperature profile was generated using the NCEP/NCAR Reanalysis data, while the SRES temperature profiles were generated using simulated atmospheric data from the GFDL CM2 Global Coupled Climate Model. Both temperature profiles were generated using observational ocean data from Wroblewski (2008). Note how the surface layer of each of the climate scenarios for 2100 shows a strong negative anomaly, indicating a fresher surface layer than average. The depth at which these anomalies occur is shallower than the negative anomaly indicated by the hindcast for 2005. The surface layer for 2005 is also saltier than the three scenarios.

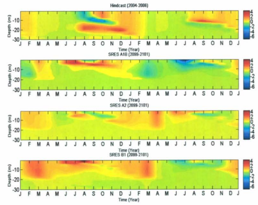

Figure 4.14. Seasonal variability of temperature (°C) anomaly for: Hindcast (2004-2006) (top panel); SRES A1B (moderate increase in GHG emissions) (2099-2101) (second panel); SRES A2 (highest increase in GHG emissions) (2099-2101) (third panel); SRES B1 (lowest increase in GHG emissions) (2099-2101) (bottom panel). These figures represent the temperature anomalies for the hindcast and the A2, A1B and B1 scenarios as generated by the GOTM. The hindcast temperature profile was generated using the NCEP/NCAR Reanalysis data, while the SRES temperature profiles were generated using simulated atmospheric data from the GFDL CM2 Global Coupled Climate Model. Both temperature profiles were generated using observational ocean data from Wroblewski (2008). Note the surface layer of each of the climate scenarios for 2100 show a negative anomaly, indicating a colder surface layer than average. The depth at which these anomalies occur is shallower than the negative anomaly indicated by the hindcast for 2005. The surface layer for 2005 is also deeper than the three scenarios.

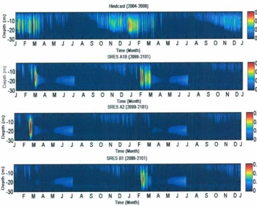

Figure 4.15. Seasonal variability of heat diffusivity (m^2/s) for: Hindcast (2004-2006) (top panel); SRES A1B (moderate increase in GHG emissions) (2099-2101) (second panel); SRES A2 (highest increase in GHG emissions) (2099-2101) (third panel); SRES B1 (lowest increase in GHG emissions) (2099-2101) (bottom panel). These figures represent the heat diffusivity profiles for the hindcast and the three future climate scenarios as generated by the GOTM. The hindcast heat diffusivity profile was generated using the NCEP/NCAR Reanalysis data, while the SRES heat diffusivity profiles were generated using simulated atmospheric data from the GFDL CM2 Global Coupled Climate Model. Both profiles were generated usingbobservational ocean data from Wroblewski (2008). Note the difference in duration, magnitude and depth of the vertical mixing for all three scenarios. There is little intense vertical mixing during winter for the A2 scenario. All three future scenarios show deep mixing during May to July.

4.5 Summary

Three atmospheric parameters of the Gilbert Bay region for three SRES were described and compared to the hindcast scenario (Chapter 3). All three scenarios indicated a warming climate over the period 2001-2101, with the greatest amount of change occurring for the A2 (highest increase in GHG emissions) scenario (Figures 4.5, 4.6). The three scenarios also suggest an increase of relative humidity during late spring and summer and a significant increase of total cloud cover (4.7, 4.8). While the SRES and ocean model simulations suggest that the future climate changes may have a strong impact on the physical environment in Gilbert Bay, the analysis (see section 4.3) indicates that these results should be considered with caution. The surface air temperature, humidity and total cloud cover show a significant bias in seasonal variability for all three scenarios. While the SRES simulations modelled by the GFDL CM2 Global Coupled Model present the best present day estimations of the future climate change, more studies are needed to improve these simulations and provide a better assessment of atmospheric characteristics.

Assessing the change of surface forcing variability on the seawater properties of Gilbert Bay for the period 2001-2101, the three SRES suggest a decrease in sea-ice thickness and duration. The SRES with higher GHG emissions suggested multiple years having little or no sea-ice, specifically the A2 (highest increase in GHG emissions) and A1B (moderate increase in GHG emissions) scenarios (Figure 4.9, 4.10). The A2 (highest increase in GHG emissions) scenario shows the strongest rate of decrease in sea-ice thickness while the B1 (lowest increase in GHG emissions) shows the weakest rate of decrease. This is a result of warming atmospheric temperatures due to increasing GHG emissions.

The change in temperature and salinity seasonal evolution for the three scenarios for 2100 was examined and compare with the hindcast scenario for 2005 (Figures 4.11, 4.12). The future projections suggest a shallower halocline and thermocline with a fresher and warmer surface layer due to increased relative humidity during late spring-summer months and increased precipitation. The study also suggests a change in the structure of vertical mixing within Gilbert Bay, with a decrease in depth and magnitude of mixing during the winter and deep mixing within the water column occurring during the late spring and summer. The decrease of intense mixing during the winter is related to a decrease in sea-ice thickness and duration and increased duration of surface cooling to the atmosphere. Scenario A2 (highest increase in GHG emissions) exhibits the greatest decrease in vertical mixing, with very little intense mixing during the winter season. The deep water mixing related to the shallow thermocline causing instability in the water column due to solar radiation penetrating past the surface mixed layer.

Overall results indicate that all future climate scenarios predict significant changes to both the atmospheric characteristics and ocean variability for Gilbert Bay for the period 2001-2101. However, the A2 (highest increase in GHG emissions) scenario predicts the most significant changes in atmospheric temperature, vertical mixing and sea-ice thickness; a result of significant GHG emissions (Figure 4.1) over the course of the century.

Chapter 5: Discussion

Results of the study indicate that atmospheric and ocean characteristics of Gilbert Bay, Labrador follow the NAO index, with warmer, wetter climates during a negative NAO and colder and drier climates during a positive NAO. This connection was apparent for the entire period 1949-2006 with the exception of the period 1995-2005, when a warming trend in the local climate of coastal Labrador occurred. During this decadal warming period, cold years as described by the NAO index exhibited both atmospheric and ocean variability characteristic of warm years. This variability of water characteristics may be considered as an example of the response of the water column to decadal warming; a result perhaps due to regional warming from the NAO and AO or perhaps a direct response to global warming. Thus, in the last decade of the hindcast scenario there appears a warming of the water column and decrease in sea-ice formation. Salinity of the surface layer also increased.

Projecting for the period 2001-2101 using three SRES, results suggest an overall warming of the climate for Gilbert Bay, Labrador. Increasing GHG emissions are linked to warming atmospheric temperatures. An increase in atmospheric temperature between 2 to 4°C for all three future climate scenarios occurred in the model predictions, with the A2 (highest increase in GHG emissions) scenario having the greatest increase in temperature. All three scenarios also suggest an increase in relative humidity during the late spring-summer months and an overall increase in total cloud cover, driven by parameters from the GFDL CM 2.0 Global Coupled Climate Model. However, if Gilbert Bay were to exhibit a climate where these changes existed, change will occur in the ocean variability. There is a significant decrease in landfast ice formation and thickness over the course of the century. The B1 (lowest increase in GHG emissions) experienced the slowest rate of decrease in thickness and duration, a potential result of the already low increase in GHG emissions (as compared to the other two scenarios) decreasing after the year 2050. The scenarios A2 (highest increase in GHG emissions) and A1B (moderate increase in GHG emissions) indicated a greater decrease in sea-ice thickness and duration with both indicating multiple years of little or no sea-ice formation. Both halocline and thermocline for the three climate scenarios are much shallower than seen in the hindcast scenario. The surface layer during the summer is also fresher and warmer than seen in the hindcast scenario. These changes in stratification are linked to increasing precipitation and relative humidity.

Significant changes also occur within the vertical mixing of Gilbert Bay, with a significant decrease during the winter and new deep mixing within the water column during the late spring and summer months. This decrease is most significant during winter for the A2 (highest increase in GHG emissions) scenario. These changes are a result of the decrease in sea-ice and penetration of solar radiation past the surface mixed layer.

Overall, the future climate scenarios predict significant changes to both the atmospheric characteristics and ocean variability for Gilbert Bay, with greater levels of GHG emissions into the atmosphere indicating a greater magnitude of climate change.

5.1 Implications

Both the hindcast and SRES suggest changing climate conditions for the Gilbert Bay ecosystem. These changing climate conditions for the Gilbert Bay ecosystem have biological, economic and social implications for the local cod population and communities surrounding Gilbert Bay.

5.1.1 Cod population (*Gadus morhua*)

It is known that the NAO index is connected to the timing of sea-ice break up, water temperature and the start and duration of thermal stratification (Meis et al., 2009; Weyhenmeyer et al., 1999; Gerten & Adrian, 2000; Straile & Adrian, 2000; Blenker et al., 2007). These factors affect the timing and duration of vertical mixing that occur within the bay and in turn affect the nutrient cycling (Meis et al., 2009; Sheffer, 1998; Lampert & Sommer, 2007). A negative NAO results in warmer air temperatures which causes warmer water column temperatures and an increased duration of stratification within the water column. When the halocline and thermocline occurs earlier in the year, as seen in the warmer years, the result can be an early bloom of phytoplankton due to improved light within the upper water column (Meis et al., 2009; Winder & Schindler, 2004; Peeters et al., 2007). There is also a link between the NAO and concentrations of zooplankton (Drinkwater et al., 2005), where concentrations of zooplankton increase with warming temperatures. Thus, warming temperatures experienced during the decadal period of the hindcast scenario for 1995-2005 (Figure 3.2) may affect the productivity of the bay, which can increase both the cod growth and population (Stenseth, et al., 2002).

There has been a connection made between warm temperatures (negative NAO index) to cod growth and recruitment off the coast of southern Labrador and northern Newfoundland (Drinkwater et al., 2005; Mann & Drinkwater, 1994). Another example which suggests this is the West Greenland cod stock. During the 1920s, a growth in the local cod stock was concurrent with an overall increase in the sea temperature along West Greenland; a change which has been linked to the NAO (Cushing, 1982; Parsons & Lear, 2001; Stenseth, et al., 2002). The relatively warm ocean during these years was favourable for cod growth (Stenseth, et al., 2002). Viewing the changes of the ocean variability within Gilbert Bay for each of the SRES, it can be seen that increasing GHG emissions may have a similar impact on the cod population. Over the course of the century, as GHG emissions increase there is an increase in atmospheric temperature (Figures 4.5, 4.6) which transcends down within the water column of the bay. This increase in ocean temperature, as originally seen in the hindcast scenario during the decadal warming period (Figure 3.7), may be beneficial for both cod growth and recruitment.

A significant increase in atmospheric temperature due to GHG emissions may also have negative consequences for the cod population of Gilbert Bay by increasing summer water column stratification. The three future climate scenarios all show increased stratification during the summer season with the mixed layer depth being less than 5 to 7 m in the early spring and summer, having a similar depth as the penetration of solar radiation in the seawater (Gosse & Wroblewski, 2004), indicating that the photic zone would also occur in this location. This is a result of warming of the upper surface layer (Overland et al., 2010) due to atmospheric warming, increased relative humidity and precipitation. The increase in stratification can reduce the circulation of nutrients from the bottom depth of the bay to the photic zone, which may potentially decrease the productivity of the bay, ultimately reducing the cod population (Overland et al., 2010; Pierce, 2004). However, for all three SRES during the months May to July vertical mixing occurs at deeper depths below the mixed surface layer. This vertical mixing may create conditions for a second phytoplankton bloom during the fall, which may aid in increasing productivity within the bay.

A decrease in sea-ice may also cause negative effects for the cod population. In the study of the three future climate scenarios, it appears that as GHG emissions increase, there is a significant decrease in intense vertical mixing during the winter season, a result of decreased sea-ice as discussed previously (Section 4.4). This decrease is most apparent in the A2 (highest increase in GHG emissions) scenario, where there is virtually no intense, deep vertical mixing within the bay during this time. This decrease in intense vertical mixing limits the amount of nutrient circulation within the water column (Overland et al., 2010), affecting the overall productivity within the bay, and thus the cod population. A decrease in this landfast ice may also affect productivity through changes in the seasonal timing and magnitude of runoff, which limit nutrients to the bay (Overland et al., 2010).

Overall, it seems if warming was to continue to increase over the course of the century, the stratification would strengthen and the vertical mixing would weaken to such a point that blooms within Gilbert Bay may not overlay with spawning of the cod larvae. This would present as a problem for feeding of the Atlantic cod larvae (Cushing, 1990).

5.1.2 Surrounding communities

The warming ocean conditions and decreasing sea-ice formation for Gilbert Bay have implications for local residents who use snowmobiles to travel over the bay during the winter. Williams Harbour is a community of approximately 50 people located on an island near the mouth of Gilbert Bay (Figure 1.1). There is no bridge to connect this community with the rest of the Labrador coast. During the winter the main form of transportation is by snowmobile. In order to travel on the sea-ice, the thickness should be approximately 1 m. The increase of atmospheric temperature observed within the last decade (Figure 3.2) presents the issue of warming climate conditions and thus, a decrease in the formation of sea-ice (Figure 3.2). For instance, a NAO index of -2.57 for the most recent year 2010 (Figure 3.10) matches the value for the extremely warm year 1969 (Figure 3.2). The average monthly air temperature for the winter of 2010 in the Gilbert Bay region was -5°C (Figure 3.10). The sea-ice in Gilbert Bay was so thin during the winter of 2010 that residents of Williams Harbour could not travel across the bay by snowmobile except for a few weeks in late February and early March.

An increase of atmospheric temperature was also observed from 2001-2101 (Figures 4.5, 4.6) for each of the SRES. This increase in temperature suggests a warming climate from increasing GHG emissions and thus, the issue of decreasing sea-ice formation as seen in the hindcast simulation. All three of the SRES suggest a decrease in sea-ice thickness and formation. Scenarios with greater GHG emissions, particularly the A2 (highest increase in GHG emissions) and A1B (moderate increase in GHG emissions) suggest various years for the Gilbert Bay having little or no sea-ice (Figures 4.9, 4.10).

With less formation of sea-ice during the winter months, unusually thin ice conditions increases the danger of travelling across the ice (Ford et al., 2005). In January 2006 a gentleman on snowmobile near Williams Harbour broke through the sea-ice due to thin conditions, nearly drowning, but was fortunate enough to be rescued in time (Governor General of Canada, 2008).

With sea-ice becoming too thin for travel and slob ice preventing the use of travel by boat, the remaining means of transportation from Williams Harbour to the rest of Labrador is by airplane (The Telegram, 2009). These flights last no longer than 10 minutes and are quite expensive costing almost $180.00 to travel to Port Hope Simpson from Williams Harbour (The Telegram, 2009). Currently the Newfoundland and Labrador provincial government is subsidizing fifty percent of the flight cost for community members of Williams Harbour during the winter months (The Telegram, 2009).

If this decrease in sea-ice seen during the decadal warming period in the hindcast scenario (Figure 3.4) were to continue to such magnitudes as suggested by the three future climate scenarios, alternate solutions for transportation may have to be found. Subsidized flights during winter may eventually no longer be economically feasible. This may lead to resettlement of the community or establishing a permanent connection to the rest of Labrador, such as building a bridge. Building a structure such as this may have serious implications on the Gilbert Bay ecosystem, which are not discussed in this study.

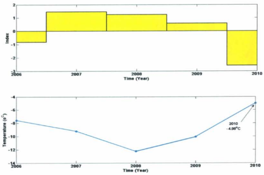

Figure 5.1. NAO index for 2006-2011. Each bar represents the NAO index for the winter months (December-March) (top panel). Mean atmospheric temperature for the winter months (December-March) of Gilbert Bay from 2006-2011. Note the very warm winter atmospheric temperature for the year 2010 (bottom panel).

Another concern with the decreasing sea-ice conditions is the way of life for aboriginal people who live on the southeastern coast of Labrador. A number of the Métis population of Labrador still use landfast ice as a form of transportation for fishing and hunting. However, with sea-ice thickness decreasing and the timing of formation and melting of sea-ice becoming less and less predictable, the relationship local people have with the sea-ice environment will change dramatically affecting their lifestyles (Laidler, 2006; Norton, 2002; George et al., 2004).

5.2 Future work and recommendations

A recommendation arising from this study is to gather more oceanographic data in Gilbert Bay, Labrador. To collect this data, it would be necessary to conduct more CTD casts in Gilbert Bay in the locations indicated in Figure 1.1. It would also be beneficial to increase the number of CTD cast locations. Doing this would not only allow for more up-to-date temperature and salinity profiles of the bay, but increasing the number of CTD cast locations would also allow for a more accurate analysis of the seasonal and interannual variability of oceanographic processes within the bay.

Among the important questions that are needed to be answered in the future are determining the possible changes in the phase intensity and spatial patterns of the NAO and how they can affect sea-ice and future atmospheric climate variability in the Gilbert Bay.

Future work may include exploring the timing and duration of greater and lesser vertical stratifications and how this links with the timing and duration of the blooms of zooplankton within Gilbert Bay. This would allow for understanding what conditions are more suitable for large blooms, as well as how these conditions have changed over time and will possibly change in the future. From this the potential impact of feeding for the Atlantic cod population within Gilbert Bay may be further addressed. In order to carry out such work, seasonal data surrounding plankton concentrations within Gilbert Bay would need to be collected.

References

Adrian, R., Wilhelm, S. & Gerten, D. (2006). Life-history traits of lake plankton species may govern their pheonological response to climate warming. *Global Change Biology,* 12, 652-661.

Best, S., Lundrigan, S., Demirov, E. & Wroblewski, J. (2011). Interannual variability of physical oceanographic characteristics of Gilbert Bay: A Marine Protected Area in Labrador, Canada. *Journal of Marine Systems, in press.*

Blencker, T., Adrian, R., Livingstone, D.M., Jennings, E., Weyhenmeyer, G.A., George, D.G., Jankowski, T., Järvinen, M., Aonghusa, C. N., Nõges, T., Straile, D. & Teubner, K. (2007). Large-scale climatic signatures in lakes across Europe: a meta-analysis. *Global Change Biology,* 13, 1314-1326.

Burchard, H., & Baumert, H. (1995). On the performance of a mixed-layer model based on the turbulence closure. *Journal of Geophysical Research,* 100, 8523-8540.

Campbell, J. L., Mitchell, M. J., Groffman, P. M. Christenson, L. M. & Hardy, J. P. (2005). Winter in northeastern North America: a critical period for ecological processes. *Frontiers in Ecology and Environment,* 3, 314-322.

Catto, N. R., Scruton, D. A., & Ollerhead, L. M. N. (2003): The coastline of eastern Newfoundland; *Canadian Technical Report of Fisheries and Aquatic Science* 2495, catalogue no. Fs 97-6/2495E.

Czaja, A., Frankignoul, C., 2002. Observed impact of Atlantic SST anomalies on the North Atlantic Oscillation. *Journal of Climate,* 15, 606-623.

Clarke, A., Church, J., & Gould, J. (2001). Chapter 1.2: Ocean Processes and Climate Phenomena. In G. Siedler, J. Church, & J. Gould, *Ocean Circulation & Climate,* 11-30. London: Academic Press.

Cohen, J. & Barlow, M. (2005). The NAO, the AO, and Global Warming: How Closely Related? *Journal of Climate,* 18, 4498-4513.

Colebrook, J. M. (1982). Continuous plankton records: phytoplankton, zooplankton and environment, North-East Atlantic and North Sea, 1958-1980, *Oceanologica Acta,* 5, 473–480.

Copeland, A., Bell, T., Edinger, E., Hu, L., and Wroblewski, J. (2006). Habitat Mapping in Gilbert Bay Labrador, a Marine Protected Area, Phase 1. *Contract report to Fisheries and Oceans Canada, St. John's, Newfoundland,* 68p.

Copeland, A., E. Edinger, T. Bell, P. LeBlanc, J. Wroblewski and R. Devillers. Geomorphic features and benthic habitats of a subarctic fjord: Gilbert Bay, Southern Labrador, Canada. In: P. Harris and E. Baker (eds). *Atlas of Seafloor Geomorphology as Habitat. Elsevier Publishing Co. in press.*

Cushing, D. H. (1990). Plankton production and year-class strength in fish productions – an update of the match mismatch hypothesis. *Advances in Marine Biology,* 26, 249-293.

Cushing, D. H. (1982). *Climate and Fisheries.* Academic Press. London (UK).

Drinkwater, K. F., Belgrano, A., Borja, A., Conversi, A., Edwards, M., Greene, C. H., Ottersen, G., Pershing, A. J. & Walker, H. (2003). The response of marine ecosystems to climate variability associated with the North Atlantic Oscillation. In *The North Atlantic Oscillation: Climate significance and environmental impact* (eds. J. W. Hurrell, Y. Kushnir, G. Ottersen and M. Visbeck). *Geophysical Monograph Series,* 134, 263-279.

Delworth, T. L., Broccoli, A. J., Rosati, A., Stouffer, R. J., Balaji, V., Beesley, J. A., Cooke, W. F., Dixon, K. W., Dunne, J., Dunne, K. A., Durachta, J. W., Findell, K. L., Ginoux, P., Gnanadesikan, A., Gordon, C. T., Griffies, S. M., Gudgel, R., Harrison, M. J., Held, I. M., Hemler, R. S., Horowitz, L. W., Klein, S. A., Knutson, T. R., Kushner, P. J., Langenhorst, A. R., Lee, H., Lin, S., Lu, J., Malyshev, S. L., Milly, P. C. D., Ramaswamy, V., Russell, J., Schwarzkopf, M. D., Shevliakova, E. A., Sirutis, J. J., Stern, W. F., Winton, M., Wittenberg, A. T., Wyman, B., Zeng, F. & Zhang, R. (2006). GFDL's CM2 Global Coupled Climate Models. Part I: Formulation and Simulation Characteristics. *Journal of Climate – Special Section/ American Meteorological Society,* 19, 643-674.

Deser, C., Walsh, J. E. & Timlin, M.S. (2000). Arctic sea ice variability in the context of recent atmospheric circulation trends, *Journal of Climate*, 13, 617– 633.

Deser, C., Holland, M., Reverdin, G. & Timlin, M. (2002). Decadal variations in Labrador Sea ice cover and North Atlantic sea surface temperatures. *Journal of Geophysical Research*, 107, 1-12.

Eicken, H., Shapiro, L. H., Gaylord, A. G., Mahoney, A., & Cotter, P. W. (2006). Mapping and Characterization of Recurring Spring Leads and Landfast Ice in the Beaufort and Chukchi Seas. *U.S. Department of the Interior Minerals Management Service (MMS) Alaska Outer Continental Shelf Region. (*Anchorage, Alaska)

Environment Canada (1993): Canada Climate normals, 1980-1990; Retrieved, December 2010, from Environment Canada, Atmosphere Environment Service: http://climate.weatheroffice.ec.gc.ca/climate_normals/index_e.html

Environment Canada (2005a): Canada Climate normals, 1990-2000; Retrieved, December 2010, from Environment Canada, Atmosphere Environment Service: http://climate.weatheroffice.ec.gc.ca/climate_normals/index_e.html

Environment Canada. (2005, September 26). CGCM3 Forcing: SRES Storylines and Scenario Families. Retrieved December 2008, from Canadian Centre for Climate Modelling and Analysis: http://www.cccma.ec.gc.ca/data/cgcm3/cgcm3_forcing.shtml

Fisheries and Oceans Canada. (2007). Gilbert Bay Marine Protected Area Management Plan. DFO/2007-1291, 33p.

Ford, J. D., Smit, B., & Wandel, J. (2005). Vulnerability to climate change in the Arctic: A case study from Arctic Bay, Canada. *Global Environmental Change,* 16, 145-160.
Geophysical Fluid Dynamics Laboratory. (2005, March 10). Retrieved from CM2.0 experiments and metadata: http://nomads.gfdl.noaa.gov/CM2.X/ CM2.0/data /cm2.0 _data.html#schematic

George, J. C., Huntington, H. P., Brewster, K., Eicken, H., Norton, D., & Glenn, R. (2004). Observations on shorefast ice dynamics in Arctic Alaska and the responses on the Inupiat hunting community, *Arctic*, 57, 363-374.

Gerten, D. & Adrian, R. (2000). Climate-driven changes in spring plankton dynamics and the sensitivity of shallow polymictic lakes to the North Atlantic Oscillation. *Limnology and Oceanography,* 45, 1058-1066.

Gosse, K. R. & Wroblewski, J. S. (2004). Variant colourations of Atlantic cod (*Gadus morhua*) in Newfoundland and Labrador nearshore waters. *ICES Journal of Marine Science,* 61, 752-759.

Government of Canada. (2005, September 26th). *Canadian Gazette.* Accessed May 3rd, 2010, on Oceans Act - Gilbert Bay Marine Protected Regulations: http://www.gazette.gc.ca/archives/p2/2005/2005-10-19/html/sor-dors295-eng.html

Governor General of Canada. (2008, February 28). Retrieved July 2010, from Media Archive: http://archive.gg.ca/media/doc.asp?lang=e&DocID=5292

Hallett, T.B., Coulson, T., Pilkington, J.G., Clutton-Brock, T.H., Pemberton, J.M. & Grenfell, B.T. (2004). Why large-scale slimate indices seem to predict ecological processes better than local weather. *Nature,* 430, 71-75.

Hondzo, M. & Stefan, H. G. (1993). Regional water temperature characteristics of lakes subjected to climate change. *Climate Change,* 24, 187-211.

Houghton, P.J., Ding, Y., Griggs, D.J., Noguer, M., van der Linden, P. J., Dai, X., Maskell, K., & Johnson, C. A. (2001). *Climate change 2001: the scientific basis: contribution of Working Group I to the Third Assessment Report of the Intergovernmental Panel on Climate Change*., Chapter 8. Cambridge, UK: Cambridge University Press.

Hu, L. & Wroblewski, J.S. (2009). Conserving a subpopulation of the northern Atlantic cod metapopulation with a marine protected area. *Aquatic Conservation: Marine and Freshwater Ecosystems,* 19, 178-193.

Hurrell, J. W. (1995). Decadal trends in the North Atlantic Oscillation: regional temperatures and precipitation. *Science,* 269, 676-679.

Hurrell, J. W. & Deser, C. (2010). North Atlantic climate variability: The role of the North Atlantic Oscillation. *Journal of Marine Systems* 79, 231-244.

Hurrell, J.W., Kushnir, Y., Visbeck, M. & Ottersen, G. (2003). An Overview of the North Atlantic Oscillation**.** In *The North Atlantic Oscillation: Climate significance and environmental impact,* (eds. J.W. Hurrell, Y. Kushnir, G. Ottersen and M. Visbeck). *Geophysical Monograph Series,* 134, 1-35.

Jamieson, G.S. & Levings, C.O. (2001) Marine protected areas in Canada- implications for both conservation and fisheries management. *Canadian Journal of Fisheries and Aquatic Sciences,* 58, 138-156.

IPCC, (2007). Climate Change 2007: Synthesis Report. Contribution of Working Groups I, II and III to the Fourth Assessment Report of the Intergovernmental Panel on Climate Change [Core Writing Team, Pachauri, R.K and Reisinger, A. (eds.)]. IPCC, Geneva, Switzerland, 104p.

Kalnay, E., Kanamitsu, M., Kistler, R., Collins, W., Deaven, D., Gandin, L., Iredell, M., Saha, S., White, G., Woollen, J., Zhu, Y., Chelliah, M., Ebisuzaki, W., Higgins, W., Janowiak, J., Mo, K. C., Ropelewski, C., Wang, J., Leetmaa, A., Reynolds, R., Jenne, R. & Joseph, D. (1996). The NCEP/NCAR 40-Year Reanalysis Project. *Bulletin of the American Meteorological Society,* 77(3), 437-471.

Köhler, J., Hilt, S., Adrian, R., Nicklisch, A., Kozerski, H.P. & Waltz, N. (2005). Long-term response of a shallow, moderately flushed lake to reduced external phosphorus and nitrogen loading. *Freshwater Biology,* 50, 1639-1650.

Kondo, J. (1975). Air-sea bulk transfer coefficients in diabatic conditions. *Boundary-Layer Meteorology*, 9, 91-112.

Laidler, G. J. (2006). Inuit and scientific perspectives on the relationship between sea ice and climate change: the ideal complement? *Climatic Change,* 78, 407-444.

Lampert, W. & Sommer, U. (2007). *Limnoecology.* Oxford University Press, New York.

Lazier, J., Pickart, R., & Rhines, P. (2001). Chapter 5.5: Deep Convection. In G. Siedler, J. Church, & J. Gould, *Ocean Circulation and Climate: Observing and Modelling the Global Ocean,* pp. 387-398. Academic Press. London (UK).

Livingstone, D. M. (1993). Temporal structure in deep-water temperature of four Swiss lakes: a short-term climatic change indicator? *Verhandlungen International Verein Limnology*, 25(1), 75-81.

Maberly, S.C. & Elliott, J.A. (2002). *Bassenthwaite Options for Remediation, p 38.* Centre for Ecology and Hydrology.

Mann, K. H., & Drinkwater, K. F. (1994). Environmental influences on fish and shellfish production in the Northwest Atlantic, *Environmental Review,* 2, 16–32.

Marsh, R., Josey, S. A., de Cuevas, B. A., Redbourn, L. J. & Quartly, G. D. (2008). Mechanisms for recent warming of the North Atlantic: Insights gained with an eddy-permitting model, *Journal of Geophysical Research,* 113, C04031.

Meis, S., Thackeray, S. J. & Jones, D. (2009). Effects of recent climate change on the phytoplankton phenology in a temperate lake. *Freshwater Biology,* 55, 1888-1898.

McGuffie, K., & Henderson-Sellers, A. (2005). *A Climate Modelling Primer* (3rd Edition ed.). West Sussex, England: John Wiley & Sons, Ltd.

Morris, J. C., & Green, M. J. (2002). Biological characteristics of a resident population of Atlantic cod (*Gadus morhua* L.) in southern Labrador. *ICES Journal of Marine Science,* 59, 666–678.

National Center for Atmospheric Research. (2009). *Climate Indices – Data.* Retrieved September 2009, from Climate and Global Dynamics Climate Analysis Section: http://www.cgd.ucar.edu/cas/jhurrell/indices.data.html#naopcdjfm

Norton, D. (2002). 'Coastal sea ice watch: Private confessions of a convert to indigenous knowledge.' In Krupnik, I. & Jolly, D. (eds.), *The Earth is Faster Now: Indigenous Observations of Arctic Environmental Change,* Arctic Research consortium of the United States in cooperation with the Arctic Studies Center, Smithsonian Institution, Fairbanks, pp. 126-155.

Ottersen, G., Planque, B., Belgrano, A., Post, E., Reid, P. C. & Stenseth, N. C. (2001). Ecological effects of the North Atlantic Oscillation, *Oecologia,* 128, 1–14.

Overland, J. E., Alheit, J., Bakun, A., Hurrell, J. W., Mackas, D. L., & Miller, A. J. (2010). Climate controls on marine ecosystems and fish populations. *Journal of Marine Systems,* 79, 305-315.

Parsons, L. S., & Lear, W. H. (2001). Climate variability and marine ecosystem impacts: a North Atlantic perspective. *Progress in Oceanography,* 49, 167-188.

Peeters, F., Straile, D., Lorke, A. & Livingstone, D.M. (2007). Earlier onset of the spring phytoplankton bloom in lakes of the temperate zone in warmer climate. *Global Change Biology,* 13, 1898-1909.

Pierce, D.W. (2004). Future changes in biological activity in the North Pacific due to anthropogenic forcing of the physical environment. *Climate Change,* 62, 389–418.

Portis, D. H., Walsh, J. E., Hamly, M. E. & Lamb, P. J. (2001). Seasonality of the North Atlantic Oscillation. *J. Climate*, 14, 2069–2078.

Robertson, D. M., & Ragotzkie, R. A. (1990). Changes in the thermal structure of moderate to large sized lakes in response to changes in air temperature. *Aquatic Science,* 52(4), 360-380.

Rodi, W. (1987). Examples of calculation methods for flow and mixing in stratified fluids. *Journal of Geophysical Research, 92* (C5), 5305-5328.

Ruzzante, D.E., Wroblewski, J.S., Taggart, C.T., Smedbol, R.K., Cook, D. & Goddard, S.V. (2000). Bay-scale population structure in coastal Atlantic cod in Labrador and Newfoundland, Canada. *Journal of Fish Biology,* 56, 431-447.

Scheffer, M. (1998). *Ecology of Shallow Lakes.* Chapman & Hall, London.

Semtner, A.J., (1976). A model for the thermodynamic growth of sea-ice in numerical investigations of climate, *Journal of Physical Oceanography*, 6, 379-389.

Stenseth, N.C. & Mysterud, A. (2005). Weather packages: finding the right scale and composition of climate in ecology. *Journal of Animal Ecology,* 74, 1195-1198.

Stenseth, N. C., Mysterud, A., Ottersen, G., Hurrell, J. W., Kung-Sik, C. & Mauricio, L. (2002). Ecological Effects of Climate Fluctuations. *Science*, 297, 1292-1296.

Straile, D. & Adrian, R. (2000). The North Atlantic Oscillation and plankton dynamics in two European lakes – two variations on a general theme. *Global Change Biology,* 6, 663-670.

Straile, D., Livingstone D. M., Weyhenmeyer G. A. & George, D. G. (2003). The response of freshwater ecosystems to climate variability associated with the North Atlantic Oscillation. In *The North Atlantic Oscillation: Climate significance and environmental impact* (eds. J. W. Hurrell, Y. Kushnir, G. Ottersen and M. Visbeck). *Geophysical Monograph Series*, 134, 263-279.

Straile, D. & Stenseth, N. C. (2007). The North Atlantic Oscillation and ecology: links between historical time-series, and lessons regarding future climate warming. *Climate Research,* 34, 259-262.

Sturm, M., Schimel, J., Michaelson, G., Welker, J. M., Oberbauer, S. F., Liston, G. E., Fahnestock, J. & Romanovsky, V. E. (2005). Winter biological processes could help convert Arctic tundra to shrubland. *Bioscience,* 55, 17-26.

Tang, G. L. (1991). A two-dimensional thermodynamical model for sea-ice advance and retreat in the Newfoundland marginal ice zone. *Journal of Geophysical Research,* 96, 4723-4737.

The Telegram. (2009, January 13th). *Airline travel to be subsidized for stranded Williams Harbour residents.* Retrieved July 2010, from www.thetelegram.com: http://www.thetelegram.com/index.cfm?sid=210395&sc=79

The Telegram. (2009, January 9th). Stranded Williams Harbour residents need subsidy: Jones. *Local News . Provincial,* A5.

Umlauf, L., Burchard, H., & Bolding, K. (2007). Retrieved from GOTM: Source code and Test Case Documentation: http://www.gotm.net/index.php?go= documentation

Vasseur, L, Catto, N.R. (2008). Atlantic Canada. In Lemmen, D.S., Warren, F.J., Lacroix, J., Bush, E., eds., From *Impacts to Adaptation: Canada in a Changing Climate 2007*. Natural Resources Canada, Ottawa, pp. 119-170.

Visbeck, M., Chassignet, E., Curry, R., Delworth, T., Dickson, B., & Krahmann, G. (2003). The ocean's response to North Atlantic Oscillation variability. In *The North Atlantic Oscillation: Climate significance and environmental impact* (eds. J. W. Hurrell, Y. Kushnir, G. Ottersen and M. Visbeck). G*eophysical Monograph Series,* 134, pp. 263-279.

Weyhenmeyer, G.A., Blencker, T. & Pettersson, K. (1999). Changes of the plankton spring outburst related to the North Atlantic Oscillation. *Limnology and Oceanography,* 44, 1788-1792.

Winder, M. & Schindler, D.E.. (2004). Climatic effects on the phenology of lake processes. *Global Change Biology,* 10, 1844-1856.

WMO/UNEP. (2000). IPCC Special Report: Emission Scenarios. Retrieved from: http://www.grida.no/climate/ipcc/spmpdf/sres-e.pdf

World Meteorological Organization (WMO). (1985). WMO sea-ice nomenclature, terminology, codes and illustrated glossary. WMO/DMM/BMO 259-TP-145, Secretariat of the WMO, Geneva.

Wroblewski, J. S., Kryger-Hann, L. K., Methven, D. A., & Haedrich, R. L. (2007). The fish fauna of Gilbert Bay, Labrador: a marine protected area in the Canadian subarctic coastal zone. *Journal of Marine Biological Association of the United Kingdom*, 87, 575-587.

Wroblewski, J. (2008). Ocean temperatures and salinities in Gilbert Bay, Labrador, 1996-1997 and 2004-2007. Memorial University Fisheries Oceanography Group Data Report 2008-1, 22p (available from the Centre for Newfoundland Studies, Memorial University of Newfoundland, St. John's, NL, Canada).